

ORGANIC-INORGANIC SOLAR CELL

M.Tech. Thesis

by

ASHIMA SINGH



**DISCIPLINE OF METALLURGY ENGINEERING AND
MATERIALS SCIENCE**

**INDIAN INSTITUTE OF TECHNOLOGY
INDORE**

JUNE 2017

ORGANIC-INORGANIC SOLAR CELL

A THESIS

*Submitted in partial fulfillment of the
requirements for the award of the degree*

of

Master of Technology

by

ASHIMA SINGH



**DISCIPLINE OF METALLURGY ENGINEERING
AND MATERIALS SCIENCE**

**INDIAN INSTITUTE OF TECHNOLOGY
INDORE**

JUNE 2017



INDIAN INSTITUTE OF TECHNOLOGY INDORE

CANDIDATE'S DECLARATION

I hereby certify that the work which is being presented in the thesis entitled **ORGANIC-INORGANIC SOLAR CELL** in the partial fulfillment of the requirements for the award of the degree of **MASTER OF TECHNOLOGY** and submitted in the **DISCIPLINE OF METALLURGY ENGINEERING AND MATERIALS SCIENCE, Indian Institute of Technology Indore**, is an authentic record of my own work carried out during the time period from July 2015 to June 2017 under the supervision of Dr. Parasharam M. Shirage, Associate Professor, IIT Indore

The matter presented in this thesis has not been submitted by me for the award of any other degree of this or any other institute.

**Signature of the student with date
(ASHIMA SINGH)**

This is to certify that the above statement made by the candidate is correct to the best of our knowledge.

Signature of the Supervisor of M.Tech. thesis (with date)

Dr. PARASHARAM M.SHIRAGE

ASHIMA SINGH has successfully given his/her M.Tech. Oral Examination held on **27 June 2017**.

Signature of Supervisor of M.Tech. thesis

Date:

Convener, DPGC

Date:

Signature of PSPC Member #1

Date:

Signature of PSPC Member #2

Date:

ACKNOWLEDGEMENTS

I would like to thank Dr. Parasharam Shirage for giving me the opportunity to experience this amazing adventure and guiding me in the most wonderful way possible, over the last one year. The members of the AFM group have been amazing, a special note of thanks to Amit Rana for helping me in the fabrication process analysis of results and for beneficial discussions. I am grateful to all members of AFM lab for constant motivation and entertaining discussions.

IITI has been a mesmerizing place to be in, with a wonderful community and I would like to thank all my friends for making whole journey in IITI full of joy and endless memories. A special thanks to IITI for SIC facility for providing FE-SEM and XRD characterizations. I am also grateful to Dr. S.R.Jadkar (Professor, Physics Department, Savitribai Phule Pune University) for providing the facility of Solar Simulator in Energy Studies lab. Last but not least, I would like to thank my parents, sister and grandparents for their support. Without their support whole journey was not so easy.

Dedicated to My Family

Abstract

The need of energy has increased tremendously in previous years due to industrial, economic development and increase in living standards of people. Fossil fuels are depleting fast due to huge amount of consumption and therefore renewable energy is need of the hour. The sun is one of the most reliable, sustainable and long term source of energy. Solar cells convert solar energy into electricity and are based on photovoltaic effect. Many types of solar cells are under research and development and at present single crystalline solar cells with PCE of 30% are widely used for converting solar energy into commercially available electricity but it has high manufacturing cost. Another type of direct bandgap and high PCE based solar cell is gallium arsenide but material cost is too high. Therefore development of new solar cell technologies with low production cost through use of inexpensive and abundant materials is need of the hour. DSCs and Organic-Inorganic Perovskite solar cells overcome the above mentioned drawbacks.

Methylammonium Lead Iodide($\text{CH}_3\text{NH}_3\text{PbI}_3$) is the perovskite which satisfies all the requirement of an efficient light harvesting materials in the cell structure. The reported efficiency of cell with this perovskite is upto 20%. Major drawback of the Perovskite solar cell is the presence Lead in the light harvester layer which is toxic in nature, another drawback is the instability in presence of humidity and high temperatures. The structure of our cell is FTO/ TiO_2 nanorods/MAPI/HTM/Al.

With the goal of fabricating stable and less toxic perovskite we studied the performance of solar cells fabricated with light harvester as Methylammonium Bismuth Iodide ($(\text{CH}_3\text{NH}_3)_3\text{Bi}_2\text{I}_9$). This perovskite has Bismuth which is less toxic in nature and comparatively more stable in ambient conditions. The cell has following layers with Bismuth based perovskite as light harvesting layer, FTO/ TiO_2 nanorods/MABI/Spiro-MeOTAD/Au. The efficiency of this cell was calculated after one week of fabrication and it showed 0.124% efficiency.

Contents

Abstract	i
List of Figures	iii
List of Abbreviations	vi
1 Introduction	1
1.1 Motivation	1
1.2 Objectives	2
1.3 Global Energy Crisis	2
1.4 Solar Photovoltaics	5
1.5 Basic Structure and Working of Solar Cell	6
1.6 Generations of Solar Cell	9
1.7 Literature Survey	12
1.8 Organisation Of Thesis	13
2 Perovskite Solar Cell	14
2.1 Introduction	14
2.2 Dye-Sensitized Solar Cell	15
2.3 Perovskite Solar Cell	18
3 Fabrication of Solar Cell	26
3.1 Introduction	26
3.2 Cleaning of FTO Substrate	27
3.3 Synthesis of TiO ₂	28
3.3.1 Synthesis of TiO ₂ Nanorods by Hydrothermal Method	28
3.3.2 Synthesis of TiO ₂ powder by Sol-Gel Method	28
3.4 Synthesis of Perovskite	29
3.4.1 Synthesis of (CH ₃ NH ₃ I)	29
3.4.2 Two step synthesis of (CH ₃ NH ₃)PbI ₃ thin film	29
3.4.3 One Step synthesis of (CH ₃ NH ₃) ₃ Bi ₂ I ₉ thin film	30
3.5 Deposition of HTM	31
3.6 Deposition of metal electrode	31
4 Results and Discussion	32
4.1 Analysis of different phases of ETL	32
4.1.1 XRD Pattern of TiO ₂ (Anatase Phase)	32
4.1.2 SEM of TiO ₂ Anatase Phase	34
4.1.3 XRD Pattern of TiO ₂ (Rutile Phase) Nanorods	35

4.1.4	TEM analysis of TiO ₂ Nanorods	36
4.1.5	SAED analysis of TiO ₂ Nanorods	36
4.1.6	FE-SEM of TiO ₂ Nanorods	37
4.2	Light Harvesting Layers	38
4.2.1	XRD analysis of CH ₃ NH ₃ I and (CH ₃ NH ₃) ₃ Bi ₂ I ₉	38
4.2.2	FE-SEM of (CH ₃ NH ₃) ₃ Bi ₂ I ₉	40
4.2.3	Efficiency Calculation of Solar Cells	41
5	Summary, Conclusions and Future Scope	44
5.1	Summary and Conclusions	44
5.2	Future Scope	45
	Appendix	46
	References	50

List of Figures

1.1	Energy requirement for electricity from 2012 to 2040 [3]	3
1.2	(a)Solar Photovoltaics annual additions and global capacity (b) Share of top 10 countries and rest of the world [4]	6
1.3	Generation of electricity in p-n junction due to Photovoltaic Effect . .	7
1.4	Basic Strucutre of (a) <i>n-i-p</i> and (b) <i>p-i-n</i> Solar Cell	8
1.5	Band Strucutre of <i>n-i-p</i> Solar Cell	8
1.6	Basic Strucutre of(a) Polycrystalline Silicon Solar Cell (b) Monocrystalline Silicon Solar Cell	10
2.1	Best Research Cell Efficiency[15]	15
2.2	Basic Structure of DSSC	16
2.3	Working of DSSC	17
2.4	Crystal Structure and Unit cell of $\text{CH}_3\text{NH}_3\text{PbI}_3$ [17]	19
2.5	(a)n-i-p structure of Perovskite Solar Cell (b)p-i-n structure of Perovskite Solar Cell	19
2.6	(a)Band Energy diagram of the n-i-p Perovskite Solar Cell (b)Band Energy diagram of the p-i-n Perovskite Solar Cell	20
2.7	(a)TEM image of TiO_2 nanoparticles prepared by hydrothermal method (b)TEM image of TiO_2 nanoparticle prepared by sol-gel method (c)SEM image of TiO_2 nanorods (d)TEM image of TiO_2 nanotubes grown by hydrothermal method (e)SEM image of nanotubes (f)Nanotubes grown on Ti sputtered on TCO (g) SEM image of 3-D photoanodes (h) Bamboo type nanostructures (i)SEM image of nanopores grown by electrochemical anodization [19]	22
2.8	Crystal structure of $(\text{CH}_3\text{NH}_3)_2\text{Bi}_2\text{I}_9$ where cyan is Bismuth, violet is Iodine,red is Nitrogen, green is Hydrogen and yellow is carbon atoms m[17]	24
3.1	n-i-p structure of Solar Cell	27
3.2	2-step Synthesis of $\text{CH}_3\text{NH}_3\text{PbI}_3$ film on TiO_2 [27]	30
3.3	Solution of $(\text{CH}_3\text{NH}_3)_2\text{Bi}_2\text{I}_9$	30
3.4	(a)Thermal Evaporation System (b)Mask used for depositing metal electrode(c)Final Solar Cell	31
4.1	XRD Pattern of TiO_2 (Anatase Phase) Nanoparticles	32
4.2	SEM image of anatase phase TiO_2 Powder (a)7.05KX (b)14.99KX . .	34
4.3	XRD pattern of TiO_2 (Rutile Phase) Nanorods	35
4.4	(a) TEM image of TiO_2 Nanorod (b) Surface Morphology	36
4.5	(a)	37

4.6	Nanorods of average width 114.24 nm in the $\text{TiO}_2/\text{TiO}_2$ Nanorods . . .	37
4.7	SEM image of TiO_2 (rutile phase) Nanorod (a) Morphology of film on FTO (b) Flower like structure made of nanorods	38
4.8	XRD Pattern of $\text{CH}_3\text{NH}_3\text{I}$	38
4.9	XRD Pattern of Bismuth based Perovskite $(\text{CH}_3\text{NH}_3)_3\text{Bi}_2\text{I}_9$ TiO_2 Nanoparticles	39
4.10	FE-SEM analysis of $(\text{CH}_3\text{NH}_3)_3\text{Bi}_2\text{I}_9$ (a) Surface Morphology of Bismuth based perovskite (b) Dimensions of hexagonal plate	40
4.11	Structure of Solar Cell	41
4.12	Efficiency calculations of solar cell with MAPI as light harvester (a)Power Density Graph (b) J - V graph of solar cell	41
4.13	(a)Presence of PbI_2 after degradation (b) $\text{CH}_3\text{NH}_3\text{PbI}_3$ Perovskite on FTO/ TiO_2	42
4.14	Structure of Solar Cell	43
4.15	Efficiency calculations of solar cell with MABI as light harvester (a) J - V graph of solar cell(b)Power Density Graph	43
5.1	Solar irradiance spectrum above the atmosphere and at the surface . .	47
5.2	MAXimum Power for I-V sweep	48
5.3	FF from I-V sweep	49

List of Abbreviations

DSSC	Dye Sensitized Solar Cell
DI	Deionized
DMF	Dimethylformamide
DMSO	N,N-Dimethyl Sulfoxide
ETL	Electron Transport Layer
FF	Fill Factor
FTO	Fluorine Doped Tin Oxide
FE-SEM	Field Emission Scanning Electron Microscope
HRTEM	High-resolution transmission electron microscopy
HTM	Hole Transport Material
ITO	Indium Doped Tin Oxide
Li-TFSI	Bis(trifluoromethane)sulfonimide lithium
MAI	Methylammonium Iodide
MABI	Methylammonium Bismuth Iodide
MAPI	Methylammonium Lead Iodide
PCE	Power Conversion Efficiency
PSC	Perovskite Solar Cell
TCO	Transparent Conductive Oxide
TBP	Tributyl Phosphate

Chapter 1

Introduction

1.1 Motivation

Exploration of better source of energy is a major field of research nowadays, and nanotechnology has unfolded new ways for development in this field. At present silicon solar cells are commercially available for generating electricity but many new technologies are under development which may help overcome the limitations of silicon solar cell. Nanotechnology is contributing to many answers towards a more sustainable, stable and eco-friendly ways to develop a photovoltaic device. Following parameters influence the performance of a photovoltaic device:

1. Efficiency
2. Stability
3. Cost of Manufacturing
4. Effect on ecosystem

Silicon solar cells are efficient and stable but due to high cost of manufacturing every section of society can't afford it, therefore there is need for new technologies which fulfil all of the above criteria. Organic-Inorganic Solar Cells can be the new revolutionary device, these were invented in year 2012[1] and since then they have reached the efficiency of 22% rapidly. The factors of stability and toxicity[2] are of major concern because these cells no matter how much efficient cannot be commercialised

if they are threat to ecosystem and human health therefore we have worked towards improving stability and reducing toxicity.

1.2 Objectives

This thesis introduces Perovskite Solar Cells with following structure FTO/TiO₂ nanorods/MA(P/B)I/(Al). The objectives to be obtained are:

1. Fabrication of stable and high efficiency solar cell
2. To use different kind of fabrication process which can done at room temperature and use precursors which are abundant in nature
3. To synthesize non-toxic perovskite material

1.3 Global Energy Crisis

Industrialization and population growth around the globe has resulted in exponential increase in demand for energy. To meet the current requirements fossil fuels are the major source as shown in Figure 1.1. Coal, natural gas and oil/petroleum are three types of fossil fuels which are used to generate energy, but their over-expenditure has caused serious environmental issues such as air pollution. Toxic gases such as carbon dioxide, nitrogen dioxide, sulphur dioxide, carbon monoxide etc. are released in environment when fossil fuels are burnt. These gases result in severe consequences on the ecosystem. Hence, the development of carbon-free sources of energy like Hydropower, Nuclear fission, Biomass, Wind, Geothermal, Solar and Ocean energy procured speed in recent years. Sunlight is the copious and reliable source of energy on our planet. It can be exploited to meet the current need of energy. However, the cost and efficiency of solar energy production is the significant barrier in moving towards the environmental friendly and sustainable technology.

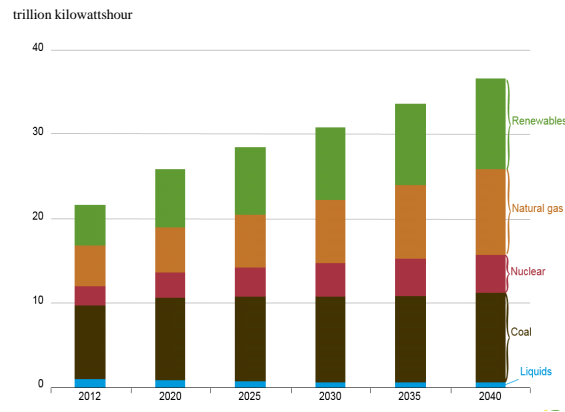


Figure 1.1: Energy requirement for electricity from 2012 to 2040 [3]

Disadvantages of Non-Renewable Sources of Energy

1. **ENVIRONMENTAL HAZARDS:** Many toxic gases are released when fossil fuels are burnt. Carbon Dioxide is one of the principal gas responsible for global warming. Hazardous results of rise in temperature of earth are melting of polar ice caps, flooding of low lying areas and rise in sea levels.

Table 1.1: CARBON DIOXIDE EQUIVALENT PER KILOWATT-HOUR (CO₂E/KWH)

Sr No	SOURCES OF ENERGY	POUNDS OF CARBON DIOXIDE EQUIVALENT PER KILOWATT-HOUR (CO ₂ E/KWH)
1	Coal	1.4 - 3.6
2	Natural Gas	0.6 - 2
3	Wind	0.02 - 0.04
4	Geothermal	0.1 - 0.2
5	Hydroelectricity	0.1 - 0.5
6	Solar	0.07 - 0.2

2. **ACID RAIN:** Sulphur dioxide is one of the pollutant that is released when fossil fuels are burnt and is a main cause of acid rain. Acid rain can lead to destruction of monuments made up of brickwork or marbles. Even crops are affected due to acidification of loams.
3. **EFFECT ON HUMAN HEALTH:** Pollution from vehicles and coal powered power plants can cause serious environmental hazards. Pollution

related diseases range from mild to severe and can significantly affect one's quality of life. Air pollution can result in asthma, chronic obstructive pulmonary disorder or COPD and lung cancer. Long-term exposure may increase respiratory infections in general population. Children and the elderly are most vulnerable to fine particulate matter and other airborne toxicants.

4. **NON-RENEWABLE:** As of today, fossil fuels are being extracted at an exorbitant rate to meet the gap between demand and supply and it is estimated that they will be finished in next 30-40 years. Since they are non-renewable, it is more likely that fuel expenses will face a steep hike in near future.
5. **IMPACT ON AQUATIC LIFE BY OIL SPILL:**Shipping of crude oil through sea cause oil spill which results in depletion of oxygen in sea. The aquatic life suffers great ordeal due to this reason
6. **COAL MINING:** Excavation of coal from areas that have huge reserves is a difficult and dangerous task. It also poses a serious health hazard to the lives of several workers who work there. The coal mining destroys wide areas of land and causes ecological imbalance.
7. **NEED HUGE AMOUNT OF RESERVES:** The coal power plants need huge and continuous supply of coal to produce required amount of energy on a constant basis. Therefore these plants require train-loads of fuel near power stations to carry out the process of generating power. This is necessary because many countries are still dependent on coal as a major source for producing power.

Advantages of Renewable Sources of Energy

1. **NO GLOBAL WARMING EMISSIONS:** Burning of fossil fuels causes overloading of greenhouse gases in our atmosphere. The release of such gases diminishes to a significant level if renewable sources are used for generation of power and energy.
2. **IMPROVED PUBLIC HEALTH AND ENVIRONMENTAL QUALITY:** Wind, solar, and hydroelectric systems generate electricity without releasing toxic gases which cause air pollution. In addition, wind and solar energy does not require water to operate which results in clean water resources. The water can be used to meet agricultural and domestic needs of people.
3. **STABLE ENERGY PRICES:** Renewable sources require one time investments to build, but once built they operate at very low cost and for most technologies the fuel is free. Due to this reason renewable energy prices are stable over time.
4. **MORE RELIABLE AND RESILIENT ENERGY SYSTEM:** Wind and solar energy modules are less prone to large-scale failure because they are distributed and modular. Distributed systems are spread out over a large geographical area, so a severe weather event in one location will not cut off power to an entire region. Modular systems are composed of numerous individual wind turbines or solar arrays. If one part of system fails then also the generation does not stop.

1.4 Solar Photovoltaics

The ever increasing need for energy to meet the modern lifestyle and the economic growth of countries has made it more important to look for new sources of energy. The best source is the Sun which provides 1500 exawatt-hours of incident energy on the earth in the form of solar radiation. This energy can be used to generate electricity and meet the requirements. The global energy generation through photovoltaics is about 303 Gigawatts as shown in Figure 1.2(a). The contribution by

countries around the world in generation of electricity through solar cells is shown in Figure 1.2(b)

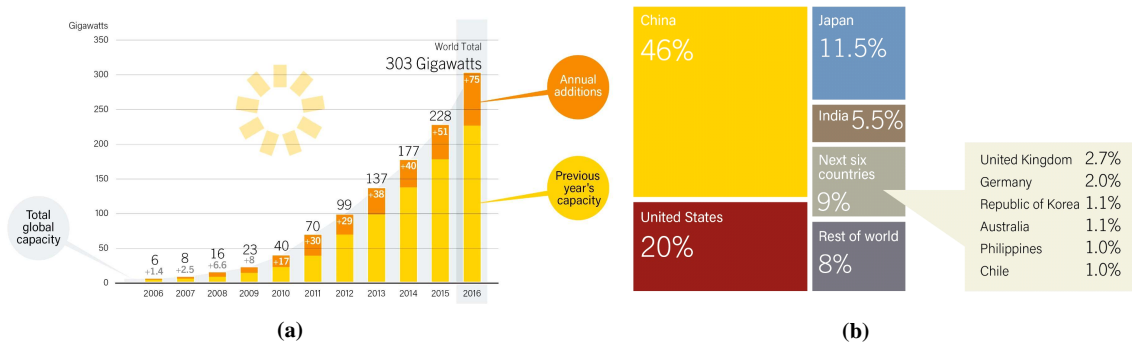


Figure 1.2: (a)Solar Photovoltaics annual additions and global capacity (b) Share of top 10 countries and rest of the world [4]

1.5 Basic Structure and Working of Solar Cell

Photovoltaic Effect

The photovoltaic effect was first discovered in 1839 by Edmond Becquerel. Basic Solar cell is made up of p-n junction in which charge separation and recombination takes place at p-n junction. The effect due to which light energy is converted to electric energy in certain semiconductor materials is known as photovoltaic effect. It generates voltage or electric current in a photovoltaic cell when it is exposed to sunlight. When photons from light source hit the p-n junction, electrons gain energy from them and thus are excited to higher energy level. Due to excitation from photons, an electron moves from the valence band to the conduction band, leaving a vacancy in the valence band. Electrons and holes in the two energy bands generate an electric field due to which voltage is generated and thus current starts flowing through the external circuit. Electrons and holes recombine in the p-n junction after generating current in the external circuit.

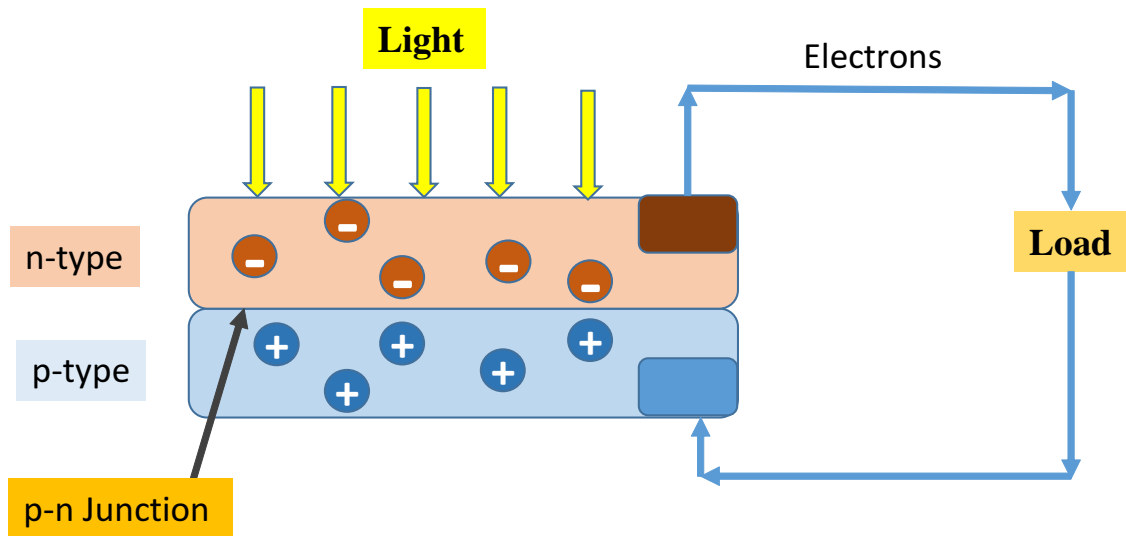


Figure 1.3: Generation of electricity in p-n junction due to Photovoltaic Effect

Structure of Basic Solar Cell

The p-n junction structure has the disadvantage of fast recombination of charges due to which there is loss of electrical energy. This disadvantage is overcome by *n-i-p* structure because in this structure it is easy to separate the photogenerated charges and prevent them from recombining. Parts of *n-i-p* and *p-i-n* Solar Cell:

1. Photoactive Layer.
2. n-doped semiconductor which is electron collector. layer
3. p-doped semiconductor which is hole collector layer.
4. Semitransparent conductive layer as electrode.
5. Metal electrode as counter-electrode. Two types of structure are possible for solar cell *n-i-p* and *p-i-n*

Working of Solar Cell

In Figure 1.4 basic structure is shown of *n-i-p* solar cell. The band structure of *n-i-p* solar cell is shown in Figure 1.5. In this cell-

1. Photoconductive Layer is Crystalline Silicon(c-Si).
2. n^+ and p^+ semiconductive layer are Amorphous Silicon(a-Si).

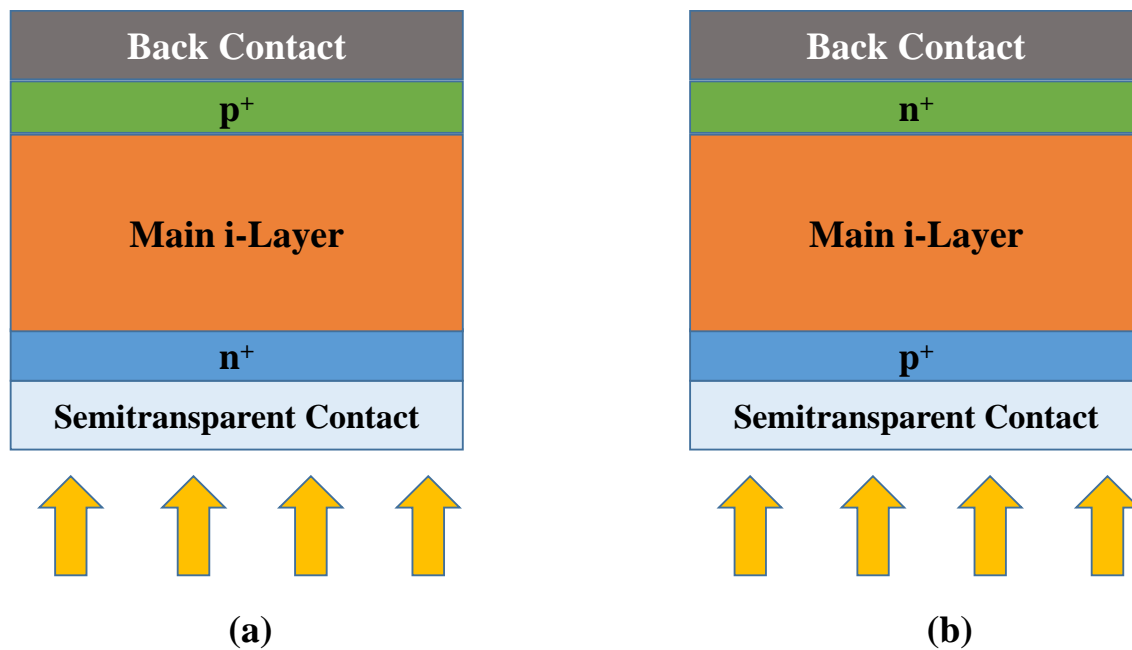


Figure 1.4: Basic Structure of (a) $n-i-p$ and (b) $p-i-n$ Solar Cell

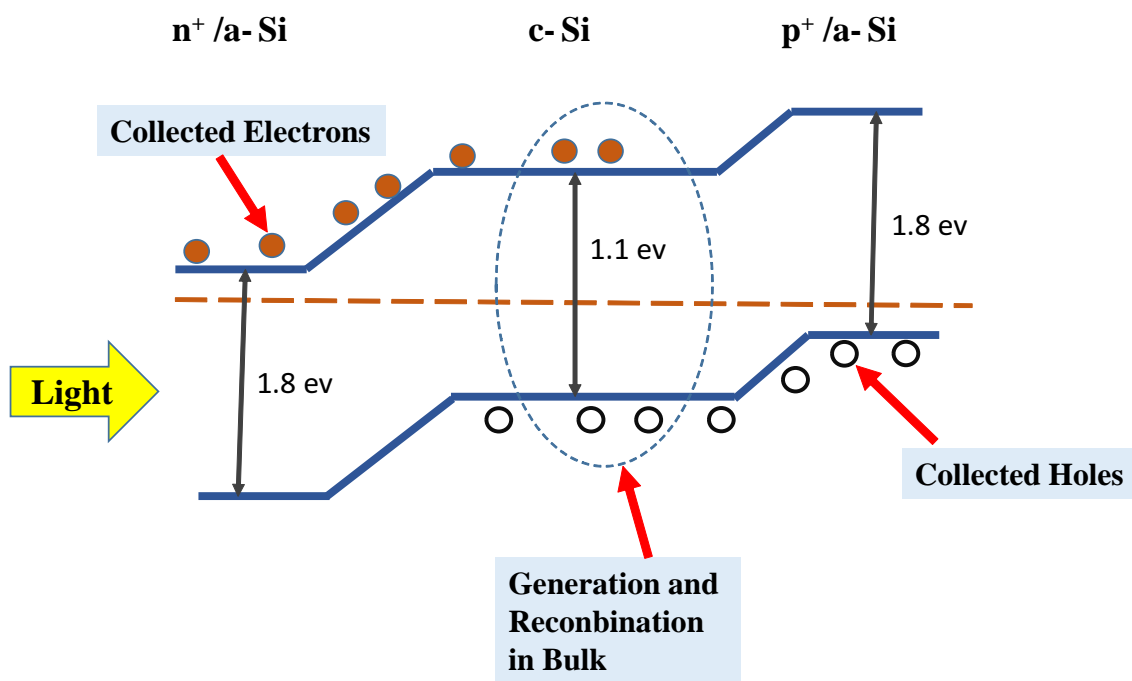


Figure 1.5: Band Structure of $n-i-p$ Solar Cell

The working of Solar Cell consist of two steps, which are as follows

1. When photons hit the photoconductive layer, electrons in the valence band move to the conduction band and leave a hole in the valence band. This is the separation of charges in the cell.

2. The electrons in the conduction band of the photoconductive layer move to the conduction band of n+-type semiconductor material and they travel to external circuit through this layer. Similarly holes move in the valence band of the p+-type semiconductor. The performance of solar cell is calculated by efficiency calculations from J-V curve obtained after simulation. The efficiency of solar cell depends on the generation and recombination of charges at p-n junction. The upper limit of efficiency of p-n junction solar cell is given by Shockley-Queisser limit[5].

1.6 Generations of Solar Cell

Solar cell technologies are traditionally divided into three generations.

First Generation

The Solar Cell of this generation are based on crystalline structure of silicon which can be of two types-

1. Monocrystal
2. Polycrystal

Polycrystalline Silicon has many grain boundaries and is made using Siemens method which requires huge amount of energy for production. It has efficiency in the range of 18-20%. Monocrystalline silicon is made by employing Czochralski method. The crystallization takes place by rotating molten silicon over seed crystal. An ingot of single crystal is formed with the crystallographic orientation governed by that of the seed crystal. The process of melting the silicon is done at 1500°C. Monocrystal shows efficiency of upto 24%. These solar cells dominate the market and are seen on rooftops. The benefits of this solar cell technology is in their good performance, as well as their high stability and the abundance of raw material for production. However, the main drawback of these solar cells is the high energy requirement for their production.



Figure 1.6: Basic Structure of (a) Polycrystalline Silicon Solar Cell (b) Monocrystalline Silicon Solar Cell

Advantages

1. These cells can last up to 25 to 30 years, thus it is cost efficient.
2. Monocrystalline solar cell is the highest efficient solar cell which is commercially available.
3. This is most stable cell up to this date in terms of humidity, heat and environmental gases.
4. It does not produce any toxic waste during its lifetime.

Disadvantages

1. The initial cost of installation of solar panels is high.
2. These cells show significant reduction in efficiency at high temperatures
3. These cannot be fabricated on flexible substrates.
4. The cost of manufacturing is high due to high energy requirements.

Second Generation:

The solar cells of this generation are based on thin film technologies. Amorphous silicon, CIGS and CdTe are some of the most developed solar cell technologies, where the typical efficiency ranges in 10 - 20%. In comparison to first generation cost of raw materials in these cells is less. Production cost is high because of vacuum process and high temperature requirements. some of the second generation solar cells are based on scarce elements and this is a limiting factor in the price.

Advantages

1. Output of these cells is less affected by temperature.
2. It is more shade tolerant *i.e* it can be efficient even in areas with less sunlight.
3. It can be fabricated on flexible substrates also.

Drawbacks

1. The a-Si solar cells have low efficiency thus they are used in devices which can operate on low energy(eg.Pocket Calculator).
2. Solar cells based on cadmium element can cause damage to environment.It can accumulate on plant and animal tissues because it is a heavy metal and potential carcinogen. The threat is minimal as long as the compound is encapsulated in the solar panel. Disposal and recycling of these cells can be hazardous and costly.

Third Generation

These are the newest type of solar cells and they show great promise towards developing highly efficient, stable and easy to manufacture cells.

1. Multijunction Solar Cells(37.5%)
2. DSSC(15%)

3. Organic Solar Cell
4. Inorganic Solar Cell
5. Organic-Inorganic Solar Cells(Perovskite Solar Cell)(22%)

The third generation technologies are causing buzz in market due to their employment to indoor facilities and in portable devices such as chargers, solar bags and solar key boards. The easy manufacturing processes and the ability to be seamlessly integrated with existing devices are reasons which are attracting industrial interest. A new thin film technology for solar cells currently under probe are perovskite solar cells. They have vast potential and have already achieved the record efficiencies beyond 22% on very small area. Polymer solar cells or plastic solar cells also have various advantages such as a simple, quick and inexpensive large-scale production and use of materials that are easily available and potentially inexpensive. Polymer solar cells can be fabricated with well-known industrial roll-to-roll (R2R) technologies that can be compared to the printing of newspapers.

1.7 Literature Survey

The DSSC cell invented by Brian O'Regan and Michael Gratzel in the year 1991 was the first step towards development of high efficiency and stable solar devices made by simple fabrication process and with elements which are abundant in nature[6]. This cell showed 12% efficiency but it had its drawbacks. The perovskite was first used in the DSSC cell by Miyasaka *et.al* as the light harvesting material[7]. But drawback of liquid electrolyte was overcome by the cell invented by Henry J Snaith *et.al* in the year 2012 which had $\text{CH}_3\text{NH}_3\text{PbI}_3$ as the light harvesting material coated on alumina mesoporous structure and Spiro-MeOTAD as the hole transport material[1]. The device showed efficiency of 10.9%. The light harvesting material with lead have been used to achieve high efficiency of upto 20.5% which is toxic in nature and is not environmental friendly[8]. Christopher N. Savory *et.al* suggested some methods to overcome the drawbacks in lead based perovskite[9]. Bismuth is one of the suitable alternative which overcomes the stability and toxicity issue of lead in perovskite material as reported by Miyasaka *et.al* and parket.al[10], [11].

1.8 Organisation Of Thesis

The thesis is organized as follows-

1. In chapter 1 overview of global energy crisis , renewable and non-renewable sources of energy , solar cell working principle and generations of solar cells are discussed.
2. In chapter 2 DSSC cell working and disadvantages are discussed,introduction to perovskite,its working principle and description of all layers is discussed.
3. In chapter 3 fabrication of the device is discussed.
4. In chapter 4 characterisations of the device fabricated by us is shown and discussed.
5. In chapter 5 conclusion and future scope is discussed.

Chapter 2

Perovskite Solar Cell

2.1 Introduction

Perovskite solar cells is an emerging photovoltaic technology which shows great potential. This technology is based on organometal halides compounds which work as light harvesting material in this device. The root of Perovskite solar cells are dye-sensitized solar cells [7]. In the year 2009 Miyasaka *et.al* made a DSSC in which adsorption of MAPI perovskite on a nanocrystalline surface (TiO_2) with a liquid electrolyte resulted in a (PCE) of around 3–4% [7]. After 2 years PCE of the cell doubled due to optimization of the perovskite coating conditions [12]. Liquid-based perovskite solar cell attracted less attention due to stability issues. It also had the drawback of instantaneous dissolution of the perovskite compound in a liquid electrolyte [13]. A long-term, stable, and high efficiency (10%) perovskite solar cell was developed in 2012 by Henry J Snaith [1]. In this cell liquid electrolyte was replaced by solid hole transport material. Efficiency of this cell structure quickly rose to 18% within 2 years [14], [15]. Since PCE values over 20% are realistically anticipated with the use of cheap organometal halide perovskite materials, perovskite solar cells are a promising photovoltaic technology [15].

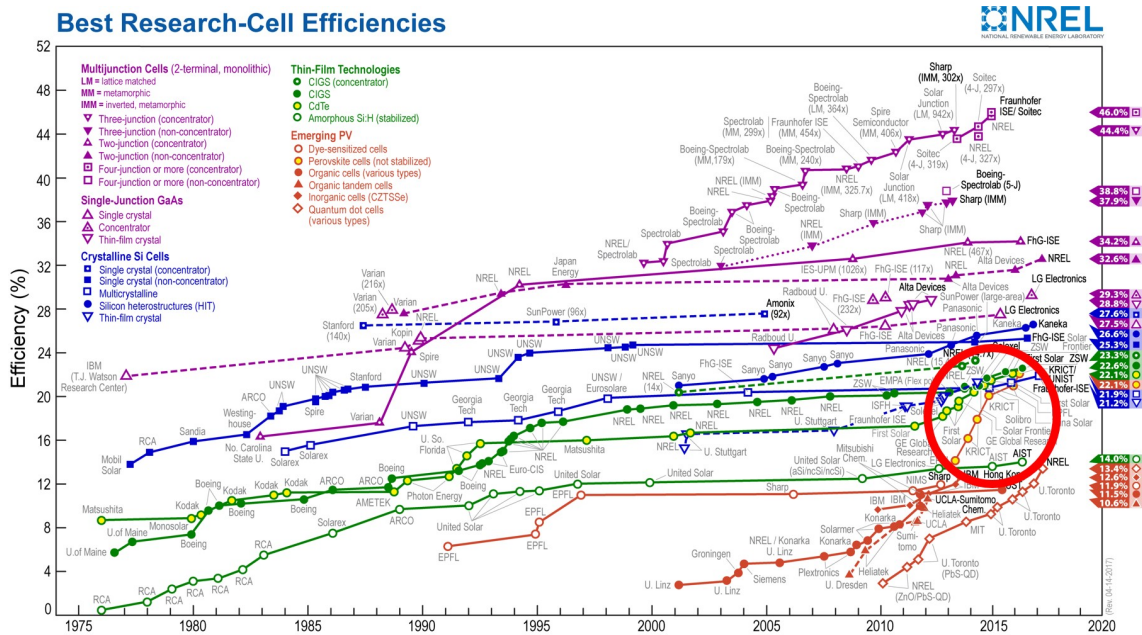


Figure 2.1: Best Research Cell Efficiency[15]

2.2 Dye-Sensitized Solar Cell

Dye Sensitized solar cell (DSSC) was invented in 1991 by Professor Michael Graetzel and Dr Brian O'Regan at École Polytechnique Fédérale de Lausanne (EPFL), Switzerland. It is also known as Graetzel Cell[6]. The first cell was only capable of using light at the ultraviolet and blue end of the spectrum but by the turn of the century, advances in technology made it possible for these cells to respond to broader spectrum of frequencies. The most efficient of the dyes were simply known as “Black dyes” due to their very dark colors. The inventors coined the term of ‘Artificial Photosynthesis’ to explain the working of this cell.

Structure

The basic structure of the Dye-sensitized solar cell is as shown in Figure 2.2 The cell has three primary parts:

1. Conducting Glass(ITO or FTO) as anode.
2. Semiconductor Oxide is deposited on the conductive side of conducting glass.
3. Photosensitive molecular sensitizers and solvent is soaked on the semiconductor oxide film which is highly porous.

4. A separate backing is made with a thin layer of the iodide electrolyte spread over a conductive sheet, typically platinum metal.

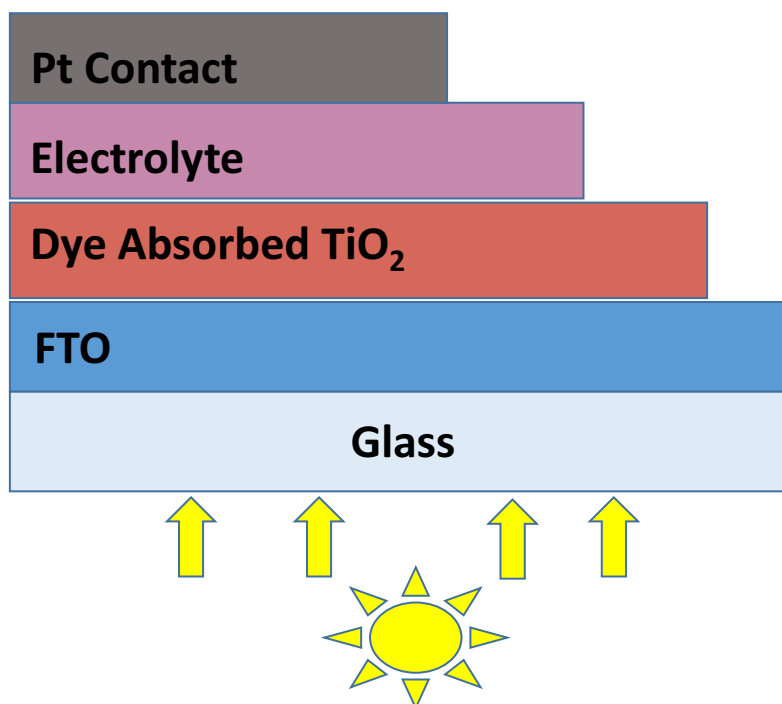


Figure 2.2: Basic Structure of DSSC

The front and back parts are then joined and sealed together to prevent the electrolyte from leaking.

Working Principle

In Dye-sensitized solid-state heterojunction solar cell, a monolayer of dye is absorbed on the surface of a mesoscopic film of TiO_2 (wide-bandgap oxide) and serves as photosensitizer. Dye absorbs light and then injects electrons into the conduction band of semiconductor oxide (the nearby TiO_2 particles). Then the electrons transport through its nanoparticle network by diffusion to the current collector (anode), subsequently pass through the external circuit, perform electrical work, and enter counter electrode (cathode). At the mean while, the dye which lost an electron starts decomposing, to replenish the dye an electron is donated by the electrolyte. Usually the electrolyte used contains iodide molecules, the iodide ion gives one electron to dye and it gets oxidized to triiodide. Cathode donates the electron to reduce triiodide to iodide ion.

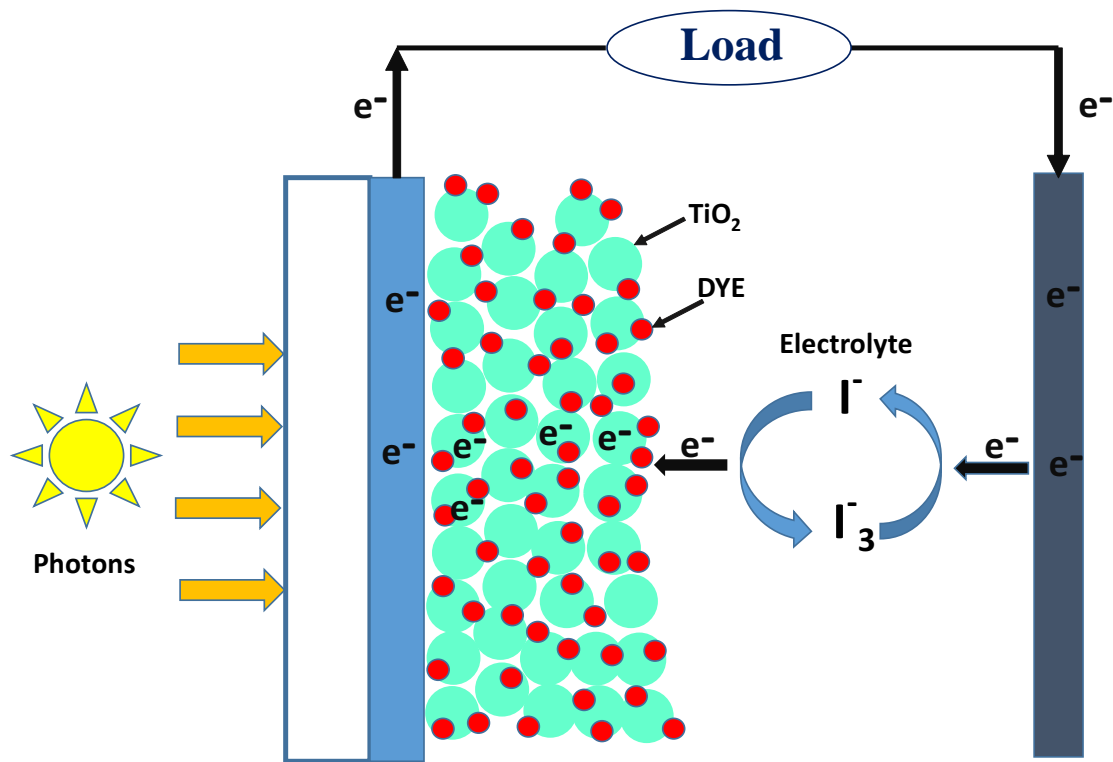


Figure 2.3: Working of DSSC

Disadvantages of DSSC

1. The major disadvantage is the requirement of liquid electrolyte in DSSCs which is temperature-sensitive. At low temperatures, the electrolyte can freeze, thus rendering the solar cell completely unusable. At high temperatures, the liquid electrolyte expands, making sealing the solar panels a major problem.
2. The use of a liquid electrolyte causes some serious additional problems such as potential instability, limitation of maximum operation temperature, danger of evaporation, and extra cost for forming an electrical series connection.
3. The volatile organic components of the electrolytic solution may leak out and therefore the dye-sensitized solar cells cannot be used for a majority of outdoor applications.

2.3 Perovskite Solar Cell

The base technology for perovskite solar cells is solid-state sensitized solar cells that are based on dye-sensitized Gratzel solar cell. This cell works exactly like DSSC, overcomes its various drawbacks and through bandgap engineering of the cell high efficiencies can be obtained [16]. This cell has become one of the major areas of research because of the following reasons

1. The fabrication process is simple and can be done at room temperature
2. The efficiency of cell can be engineered by varying any one the layers
3. The materials used in the fabrication of cell are in abundance in nature and thus this can be the option for sustainable source of energy.

Structure of Perovskite

Perovskite, named after the Russian mineralogist L.A. Perovski, has a specific crystal structure with the (ABX_3) formula (X = oxygen, halogen). The larger cation A occupies a cubo-octahedral site shared with twelve X anions while the smaller B cation is stabilized in an octahedral site shared with six X anions. perovskite containing halogen anions allow monovalent and divalent cations in A and B sites, respectively, to fulfill charge neutrality. In $CH_3NH_3PbI_3^+$, the A-site cation is CH_3NH_3 and the B-site cation is Pb_2^+ and X is a halide (I^- , Br^- , or Cl^-) as shown in Figure 2.4

Solar Cell Structure and Band Energy Diagram

Structure of the cell is as shown in Figure 2.5. It has following layers

1. **Photoconductive Layer-** Perovskite is used here which is basically made up of organic cation, metal atom and halogen. Some of the commonly used perovskites are $CH_3NH_3PbBr_3$, $CH_3NH_3PbCl_3$, $CH_3NH_3PbI_3$, $CH_3NH_3PbBr_{x-1}I_1-x$, $(CH_3NH_3)_3Bi_2I_9$

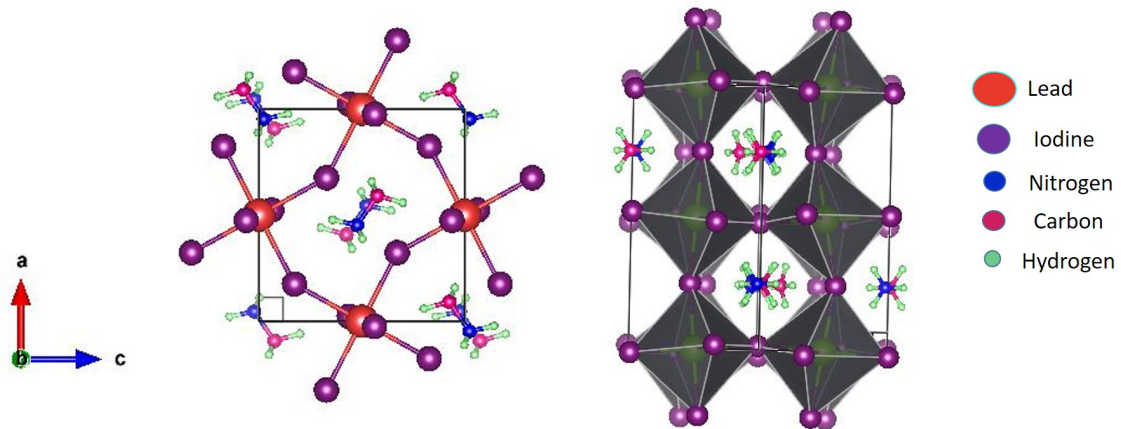


Figure 2.4: Crystal Structure and Unit cell of $\text{CH}_3\text{NH}_3\text{PbI}_3$ [17]

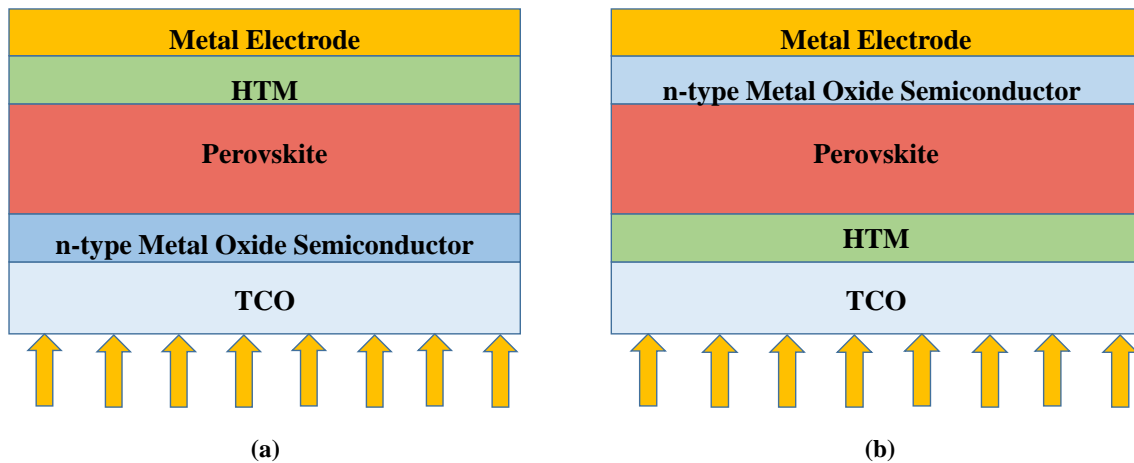


Figure 2.5: (a)n-i-p structure of Perovskite Solar Cell (b)p-i-n structure of Perovskite Solar Cell

2. **n-type Semiconductor**- Metal oxides are used as n-type semiconductors in the cell, some of them are $\text{TiO}_2, \text{ZnO}_2, \text{Al}_2\text{O}_3$. Electrons generated in the photoconductive layer travel through this layer to reach the external circuit.
3. **p-type Semiconductor**- It is also called as Hole transport material, holes generated travel through this layer. Some of the HTMs are Spiro-MeOtd, PTAA, PCDTBT, PCPDTBT, P3HT etc.
4. **Transparent Conductive Oxide**- This layer is used to transport either either electrons or holes depending on the n-i-p or the p-i-n structure respectively. This acts as electrode, ITO and FTO are mostly used for this purpose. Light enters in the cell through this layer and then reaches the photoconductive layer.

5. **Metal Electrode**- This acts as the counterelectrode and can be of Au, Ag and Al.

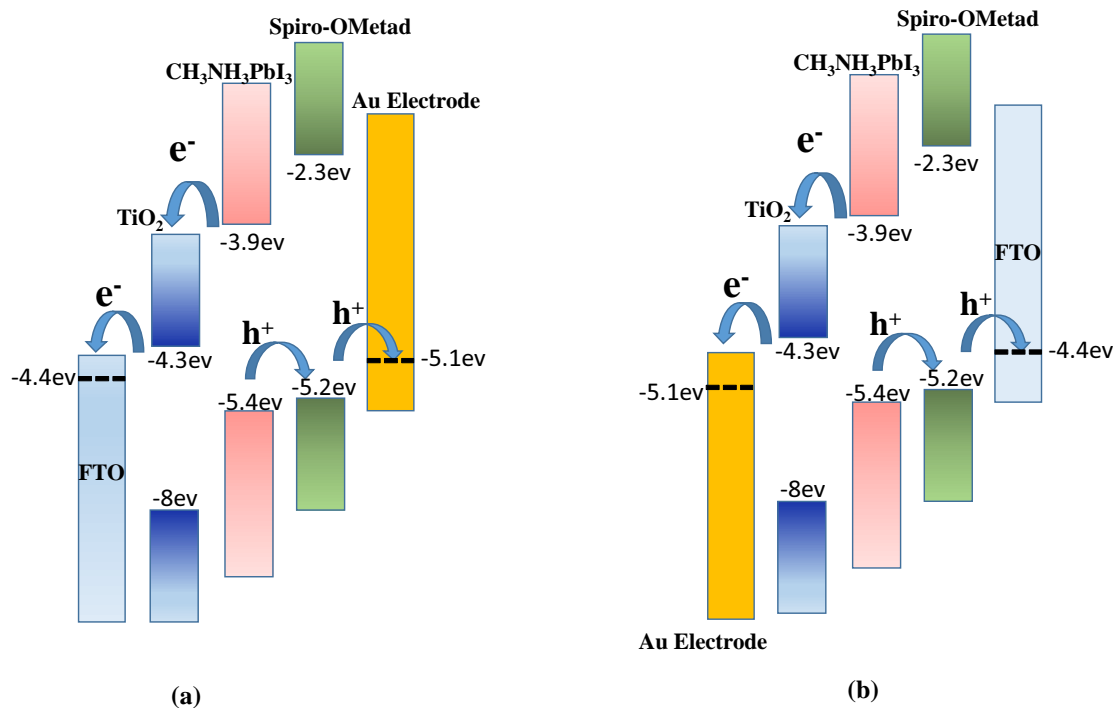


Figure 2.6: (a) Band Energy diagram of the n-i-p Perovskite Solar Cell (b) Band Energy diagram of the p-i-n Perovskite Solar Cell

Desirable band energy structure of perovskite solar cell should be as shown in Figure 2.6. Photoconductive layer is of perovskite with bandgap in the range 1.2-1.5 eV. This is the required bandgap for the photovoltaic effect to take place. The LUMO of perovskite's conduction band should be above conduction band of n-type semiconductor so that electrons can move easily from light harvesting layer to the n-type semiconductor. The HOMO of valence band of the perovskite should be less than the valence band of p-type semiconductor for the generated holes to move. Electrons travel from n-type semiconductor to the transparent conductive oxide and holes move through p-type semiconductor to the metal electrode.

Description of Layers of Cell

1. **Transparent Conductive Oxide**- It functions as a current collector and a support of the semiconductor layer in DSSC. It has two important features:

- (a) The high optical transparency which allows natural sunlight to pass through to the beneath of the active material without unwanted absorption of the solar spectrum.
- (b) Low electrical resistivity which facilitates the electron transfer process and reduces the energy loss

Current transparent conducting oxides used in industry are primarily n-type conductors. The comparison between two is shown in Table 2.1.

Table 2.1: Comparison of ITO and FTO

Sr.No	ITO	FTO
1	Cannot work well above 350°C	Works well upto 600°C
2	Medium Transparency in Visible Light	FTO surface is better transparent to visible light
3	Resistance of ITO glass substrate increases with temperature	Resistivity of FTO coated glass substrate is constant up to 600 0C
4	ITO coated glass plate has a lower thermal stability	FTO coated substrate has an excellent thermal stability
6	ITO coated sheets has moderate conductivity	FTO coated surface has a good conductivity
7	ITO coating is moderately tolerable for physical abrasion	FTO layer is high tolerance to physical abrasion
8	ITO has a cubic structure in nature	FTO consist tetragonal structure
9	ITO has a lower reflectance in infrared zone	FTO has a higher reflectance in infrared zone

The most favoured dopants for SnO₂ are antimony which substitutes the tin cations or by fluorine via substituting the oxygen atoms. Fluorine doped tin oxide (FTO) exhibits good visible transparency owing to its wide band-gap, while retaining a low electrical resistivity due to the high carrier concentration (Nd) caused by the oxygen vacancies and the substitutional fluorine dopant.

2. **Semiconductor Metal Oxide-** The choice of metal oxide can be made between different n-type oxides such as TiO₂, ZnO, SnO₂ and other ternary oxide like Zn₂SnO₄. Solar cell with efficiency of 15.7% with ETL as ZnO has been reported [18]. TiO₂ is the most abundantly used photoanode material in solar cells due to its superior characteristics. A wide variety of nanostructured TiO₂ has been used as photoanodes as reported in [19] with the aim of exploit-

ing nanoscale material properties. Several fabrication techniques like Sol-gel, Hydrothermal, Electrochemical deposition, Spin coating, Dip coating, Spray pyrolysis, Solvothermal, Chemical vapour deposition and Microwave assisted synthesis have been reported for the synthesis of TiO₂ nanostructures.

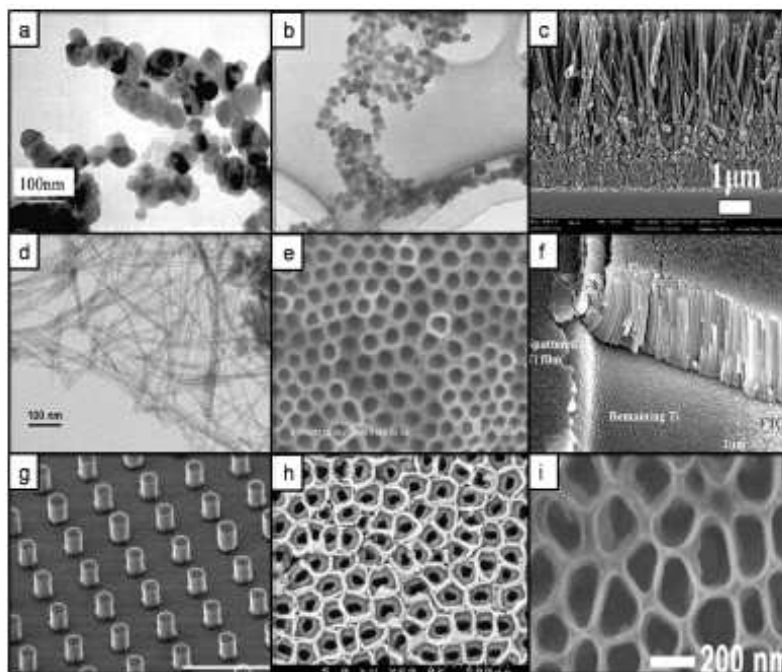


Figure 2.7: (a)TEM image of TiO₂ nanoparticles prepared by hydrothermal method (b)TEM image of TiO₂ nanoparticle prepared by sol-gel method (c)SEM image of TiO₂ nanorods (d)TEM image of TiO₂ nanotubes grown by hydrothermal method (e)SEM image of nanotubes (f)Nanotubes grown on Ti sputtered on TCO (g) SEM image of 3-D photoanodes (h) Bamboo type nanostructures (i)SEM image of nanopores grown by electrochemical anodization [19]

3. **Perovskite Layer**-Organometal halide compounds are under intensive investigation due to their ability to show rapid growth in PCE% in solar cells [20]. First time perovskite compound CH₃NH₃X(I,Br) was used by Miyasaka *et.al* [7] as a light harvester in liquid-based dye sensitized solar cells (DSSCs) in 2009, where the iodide cell showed PCE of 3.8%. Higher efficiency (6.5%) cells were made by Park *et al.* employing MAPbI₃ and iodide redox electrolyte in 2011[21]. By employing HTMs in the solar cell the instability of the MAPbX₃ in liquid electrolyte was improved. It was used as a light harvester in solid state dssc in the year 2012 by Henry J Snaith *et.al* and reported efficiency of 10.9%. Since then many groups have worked on perovskite solar cells which have reached the efficiency of about 22%. The exclusive use of widely avail-

able elements and the capacity for film deposition through either solution or vacuum-based methods is an indication of the tremendous potential of these compounds to completely redefine the way that materials are designed and chosen for electronic device applications[20].

Advantages of $\text{CH}_3\text{NH}_3\text{PbI}_3$ Perovskite

- (a) They strongly absorb sunlight over a broader range of spectrum and thus enable the thinner sensitized layer.
- (b) Long Diffusion length of $1\ \mu\text{m}$ for both the charge carriers ensures the less recombination rate[22].
- (c) High Mobility and slow recombination ensures more current generation in the cell.[23], [24]
- (d) The excellent optoelectronic properties are elucidated by the suitable direct band gap of 1.55 eV, shallow defect levels and low effective masses of the carrier[25].

Drawbacks of $\text{CH}_3\text{NH}_3\text{PbI}_3$ Perovskite

- (a) Degrades in presence of humidity due to hydrolysis of the photoconductive layer upon contact with air.
- (b) It possesses poor thermal stability and quickly decomposes at temperatures above 85°C .
- (c) Toxicity of lead is the major roadblock toward commercialisation of this cell.

Development of Bismuth based Perovskite

To overcome the above mentioned drawbacks of $\text{CH}_3\text{NH}_3\text{PbI}_2$ perovskite due to presence of lead other perovskites with the inorganic cation of $6s^2$ electronic configuration have been studied. First Sn was used to replace Pb in the

structure but it showed certain shortcomings like [2]

- (a) High recombination of charges in the bulk.
- (b) Stability in ambient condition is very poor which makes the fabrication process very typical.

Therefore we decided to study the properties of $(\text{CH}_3\text{NH}_3)_2\text{Bi}_2\text{I}_9$ which is new class of perovskites and has shown much many benefits like

- (a) High stability in ambient conditions over long period of time.
- (b) Less toxicity of Bismuth is major advantage over $\text{CH}_3\text{NH}_3\text{PbI}_2$ perovskite.

In Figure 2.8 we see the crystal structure of $(\text{CH}_3\text{NH}_3)_3\text{Bi}_2\text{I}_9$ perovskite [17], in this we observe that two bismuth atoms in the anion structure are in bond with 3 symmetrical Iodine atoms which are in bridging and terminal positions. Between two face sharing octahedra in complex anion CH_3NH_3^+ is present. In the crystal structure the anions are arranged along c-axis. This shows direct bandgap of 1.94 eV in the absorption spectra measured between 250 nm and 900 nm. [26] But it has the disadvantage of low efficiency maybe due to large direct bandgap of 2 eV, high effective mass of the charges, low mobility of the charges, rough morphology of the perovskite and band energy mismatch in the stack structure. [26]

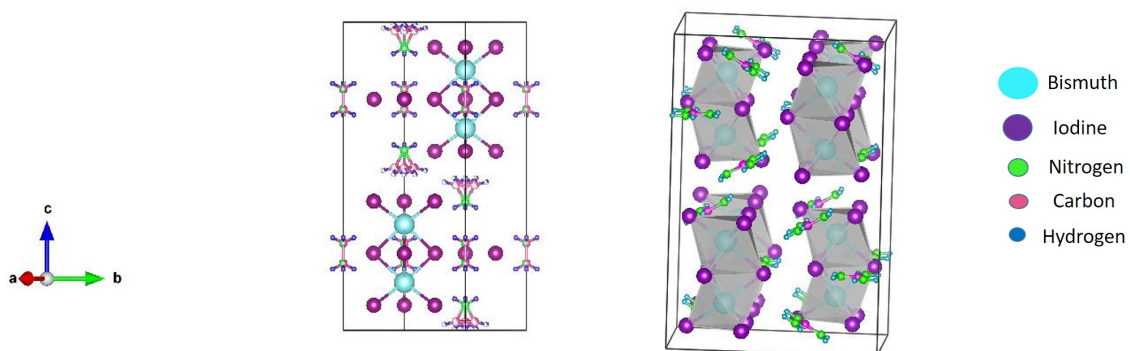


Figure 2.8: Crystal structure of $(\text{CH}_3\text{NH}_3)_2\text{Bi}_2\text{I}_9$ where cyan is Bismuth, violet is Iodine, red is Nitrogen, green is Hydrogen and yellow is carbon atoms m [17]

4. Hole Transport Material

Hole transporting materials (HTMs) in efficient PSCs with a fluorine-doped tin oxide (FTO)/blocking layer (bl)- TiO_2 /mp-

TiO₂/perovskite/HTM/Au are necessary for efficient extraction of the holes toward the Au and perfect prevention of electrons across the interface. Many researchers have demonstrated various fabrication methods for depositing perovskite-film with dense, uniform morphologies, and full surface coverage. Despite such efforts, some difficulties remain in depositing a smooth and flat perovskite film with low surface roughness on top of a mp-TiO₂ scaffold. Thus, it is crucial that the hole transporting layer should be sufficiently thick to cover the entire area of the perovskite film before deposition of metal. Many types of HTMs used in cell are Spiro-MeOTAD, PTAA, P3HT, PCPDBT, PCDTBT etc. Performance of various HTMs as reported in [16] are shown in Table 2.2

Table 2.2: Comparison of HTMs performance in CH₃NH₃PbI₃ based solar cell

HTM	Jsc($mA\ cm^{-2}$)	Voc(v)	FF(%)	PCE(%)
spiro-OMeTAD	16.7	0.855	58.8	8.4
PTAA	16.5	0.997	72.7	12
P3HT	12.6	0.73	73.2	6.7
PCPDTBT	10.3	0.7	66.7	5.3
PTAA	16.4	0.9	61.4	9
Without	6.8	0.68	53.8	2.5

5. **Metal Contacts-** Metal contacts can be made of Platinum, Gold, Silver and Aluminium for the purpose of counter electrode. Holes generated in the light harvesting layer move through the HTM and are collected in the metal electrode. These are mainly deposited through thermalevaporation process. Gold is most suitable for the spiro-OMeTAD HTM because energy level of gold is -5.1 eV and the valence band maximum of HTM is -5.2 eV which makes movement of holes easy.

Chapter 3

Fabrication of Solar Cell

3.1 Introduction

Fabrication process of Solar Cell consist of following steps

1. Cleaning of FTO Glass
2. Synthesis of TiO_2 Nanorods
3. Synthesis of Perovskite Layer
4. HTM layer Coating
5. Metal Electrode Deposition

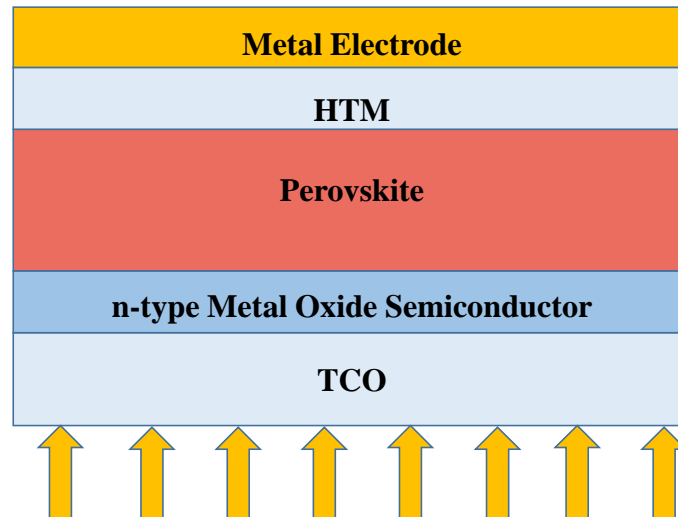


Figure 3.1: n-i-p structure of Solar Cell

Here we are fabricating solar cell of n-i-p structure, with the following layers

1. FTO as TCO
2. TiO_2 as n-type Metal Oxide Semiconductor
3. $(\text{CH}_3\text{NH}_3)\text{PbI}_3$ or $(\text{CH}_3\text{NH}_3)_3\text{Bi}_2\text{I}_9$ as Light Harvesting Layer
4. spiro-OMeTAD as HTM
5. Au or Al Metal Electrode

3.2 Cleaning of FTO Substrate

We purchased FTO glass sheet of 18x18 cm dimensions from .This is cut in 2x2 cm dimensions substrates.

1. First the substrate is ultrasonicated in ethanol for 10 minutes and then dried for 5 minutes.
2. In second step substrate is ultasonicated in isopropnol for 10 minutes and then again heated.
3. At last substrate is ultrasonicated in DI water for 10 minutes and heated in vacuum for 10 minutes.

3.3 Synthesis of TiO₂

3.3.1 Synthesis of TiO₂ Nanorods by Hydrothermal Method

Chemicals Required

1. concentrated HCL(36.5%-38% by weight)
2. Titanium Butoxide(97% Sigma Aldrich)
3. DI water

Preparation

In a typical thin film deposition on FTO glass , 1:1 (by volume) ratio of DI water and concentrated HCL(36.5%-38% by weight) are stirred at low temperatures using ice bath for 5 minutes. After stirring the mixture,48.5 mM of titanium butoxide(97% Sigma Aldrich) is added and the solution is stirred for another 5 minutes.The FTO glasses are placed vertically in Teflon lined 125 ml container with conducting side facing inwards. Autoclave is kept in furnace at temperature 150°C for a period of 4-24 hrs. After synthesis autoclave is removed from furnace and kept in ambient condition until it cools down to room temperature. FTO glasses are taken out of Teflon liner, cleaned using ethanol and dried at room temperature. Some TiO₂ coated FTO glass are annealed at 450°C for 4 hours.

3.3.2 Synthesis of TiO₂ powder by Sol-Gel Method

Chemicals Required

1. Titanium(IV) Tetrabutoxide(Sigma Aldrich)
2. Hydrogen Peroxide(H₂O₂, 30%)
3. DI water

Preparation

In the preparation of Ti-precursor sol, 0.14 M of titanium(IV) tetrabutoxide (Aldrich chemicals) was hydrolyzed with deionized water (100 ml), the resulting titanium hydroxide precipitate was separated by decantation and washed thoroughly with water until the alcohol generated during hydrolysis of titanium alkoxide was completely removed. The precipitate was dissolved in 75 ml of aqueous hydrogen peroxide (30% Qualigen-make) to get a transparent orange sol of titanium peroxo complex. The sol was diluted with water to obtain the solution of different concentrations, after dilution the color of the sol changes from orange to yellow. The gel is aged for 24 hours and then it is dried. Yellow powder of titanium peroxide is obtained which when heated below 600°C gives anatase phase TiO₂ nanoparticles

3.4 Synthesis of Perovskite

3.4.1 Synthesis of (CH₃NH₃I)

CH₃NH₃I, to be used as a light harvester, was synthesized according to method reported in [16] by reacting 27.86 ml methylamine (40% in methanol,) and 30 ml hydroiodic acid (57 wt% in water, Sigma Aldrich) in a 250 ml round-bottomed flask at 0°C for 2 h with stirring. The precipitate was recovered by evaporation at 50°C for 1 h. The product, methyl ammonium iodide CH₃NH₃I, was dissolved in ethanol, recrystallized from diethyl ether, and dried at 60°C in a vacuum oven for 24 h.

3.4.2 Two step synthesis of (CH₃NH₃)PbI₃ thin film

In 1 ml N,N-dimethylformamide (DMF, 99.8% Sigma-Aldrich), 1 M of PbI₂ was dissolved at 70°C to make 1M PbI₂ solution. Twenty microliters PbI₂ solution was spin-coated on the TiO₂ layer at 3000 rpm for 20 s and dried at 40°C for 3 min and 100°C for 5 min consecutively. One hundred microliters of 0.063M CH₃NH₃I solution in 2-propanol (Aldrich) was loaded on the PbI₂-coated substrate for 20 s, which was spun at 4000 rpm for 20 s and then dried at 100°C for 5 min. It took 4 s

to reach 4000 rpm.

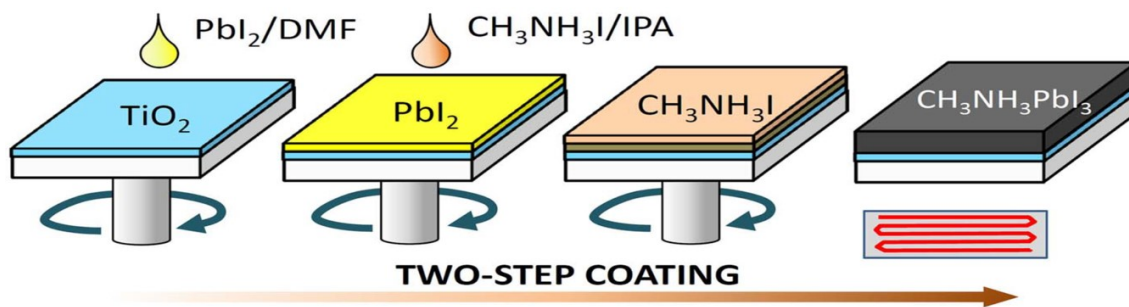


Figure 3.2: 2-step Synthesis of $\text{CH}_3\text{NH}_3\text{PbI}_3$ film on TiO_2 [27]

3.4.3 One Step synthesis of $(\text{CH}_3\text{NH}_3)_3\text{Bi}_2\text{I}_9$ thin film

This is prepared by taking 7:3 (by volume) ratio of DMF/DMSO as solvents, in this solvent 0.75 M of $\text{CH}_3\text{NH}_3\text{I}$ is dissolved and then 0.35 M of BiI_3 is dissolved. This solution is stirred for about 30 minutes on the magnetic stirrer. The prepared solution is spin coated on the TiO_2 layer at 2000 rpm for 20 seconds and then heated at 110°C for 30 minutes.



Figure 3.3: Solution of $(\text{CH}_3\text{NH}_3)_2\text{Bi}_2\text{I}_9$

3.5 Deposition of HTM

Spiro-MeOTAD solution is prepared by dissolving 59 mM of Spiro-MeOTAD in 1ml of chlorobenzene. Another solution is prepared by dissolving 1.812 M of Li-TFSI in 1mL of acetonitrile. 28.8 μL of TBP and 17.5 μL of the above prepared solution is dissolved in the Spiro-MeOTAD solution. 10 μL of the solution is then spin coated on the light harvesting layer.

3.6 Deposition of metal electrode

Alluminium contact is deposited on the HTM layer by thermal evaporation process. Final cells look as shown in the Figure3.3(c).

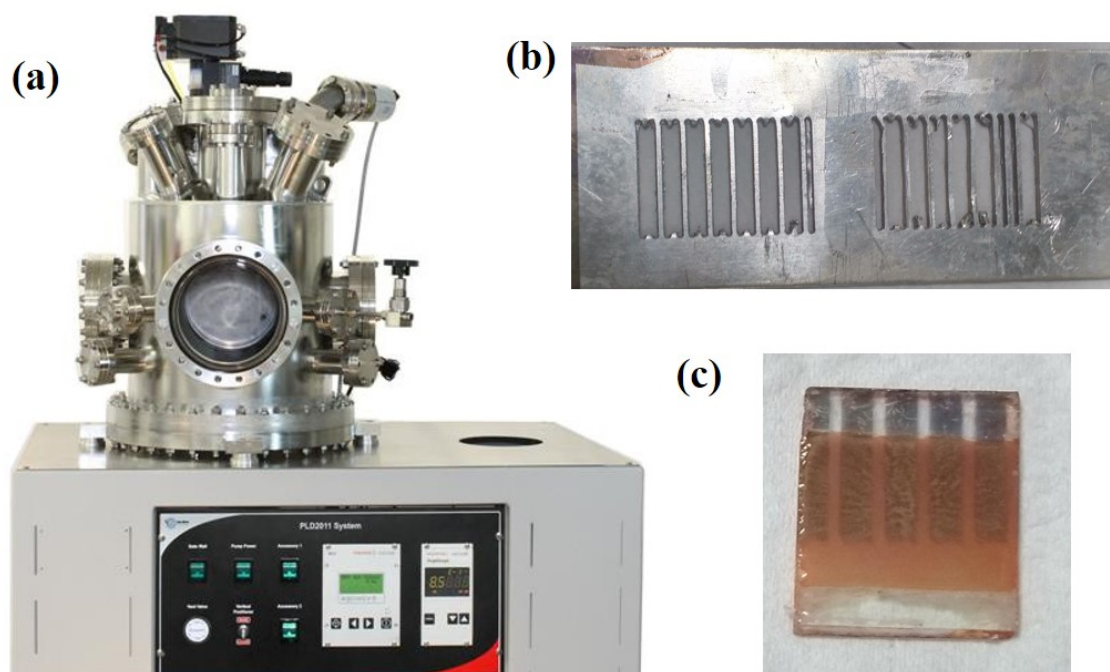


Figure 3.4: (a)Thermal Evaporation System (b)Mask used for depositing metal electrode(c)Final Solar Cell

Chapter 4

Results and Discussion

4.1 Analysis of different phases of ETL

4.1.1 XRD Pattern of TiO_2 (Anatase Phase)

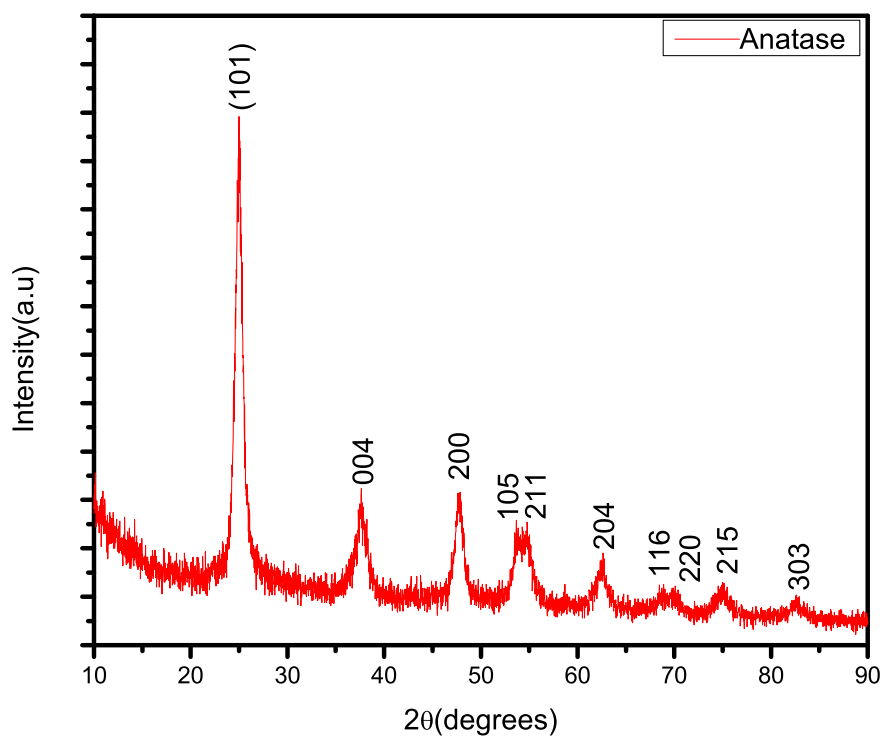


Figure 4.1: XRD Pattern of TiO_2 (Anatase Phase) Nanoparticles

XRD of all samples are done on Rigaku SmartLab, Automated Multipurpose x-ray Diffractometer, Figure 4.1 shows the X-ray diffractogram of the TiO₂ nanoparticles powder annealed at 350 °C. The determined characteristics 2θ values and [hkl] planes are as given in Table 4.1 The values are confirmed with JCPDS Card No(84-1286).

Table 4.1

Sr.No	2θ	[hkl]
1	25.01	101
2	37.59	004
3	47.79	200
4	53.69	105
5	54.81	211
6	62.62	204
7	68.61	116
8	70.57	220
9	75.03	215
10	82.696	303

From the X-ray diffraction patterns of the TiO₂ sample annealed at 350 °C for 3 h, demonstrate the formation of anatase phase . The peak at 25.01⁰ was observed [101] reflections, which is the strongest reflection for the TiO₂ polymorphs. Crystal size is calculated using Scherrer Equation and the size is 8.34 nm.

$$D = K\lambda/\beta\cos\theta$$

Common reported qualities of photoactive TiO₂ nanoparticles include high crystallinity, anatase phase material small crystallite size and small particle size . These small particles from agglomerating, whilst still providing sufficient exposed titania sites on which photocatalytic reaction can takes place . Therefore in our studies, synthesis of the TiO₂ nanoparticles was carried out at 300 °C for 3hr in ambient atmosphere.

4.1.2 SEM of TiO₂ Anatase Phase

FE-SEM analysis is done on Field-Emission Scanning Electron Microscope (FE-SEM), Supra55 Zeiss. In the Figure 4.2 we observe that TiO₂ nanoparticles that are formed have agglomerated and formed particles of μm size. But the anatase phase is confirmed by the XRD analysis. Agglomeration can be due to the process of synthesis, temperature variations or precursor's proportion in the synthesis process. From here the calculated particle size is

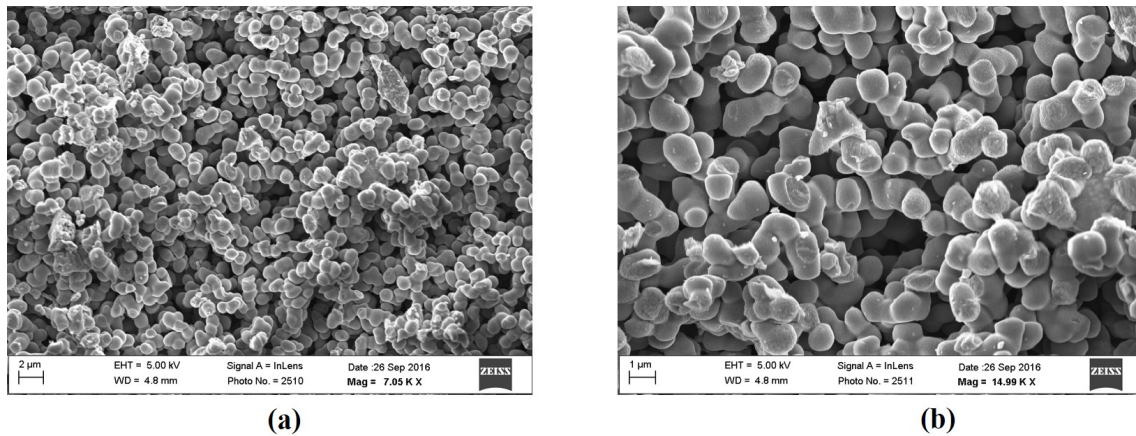


Figure 4.2: SEM image of anatase phase TiO₂ Powder (a)7.05KX (b)14.99KX

4.1.3 XRD Pattern of TiO₂(Rutile Phase) Nanorods

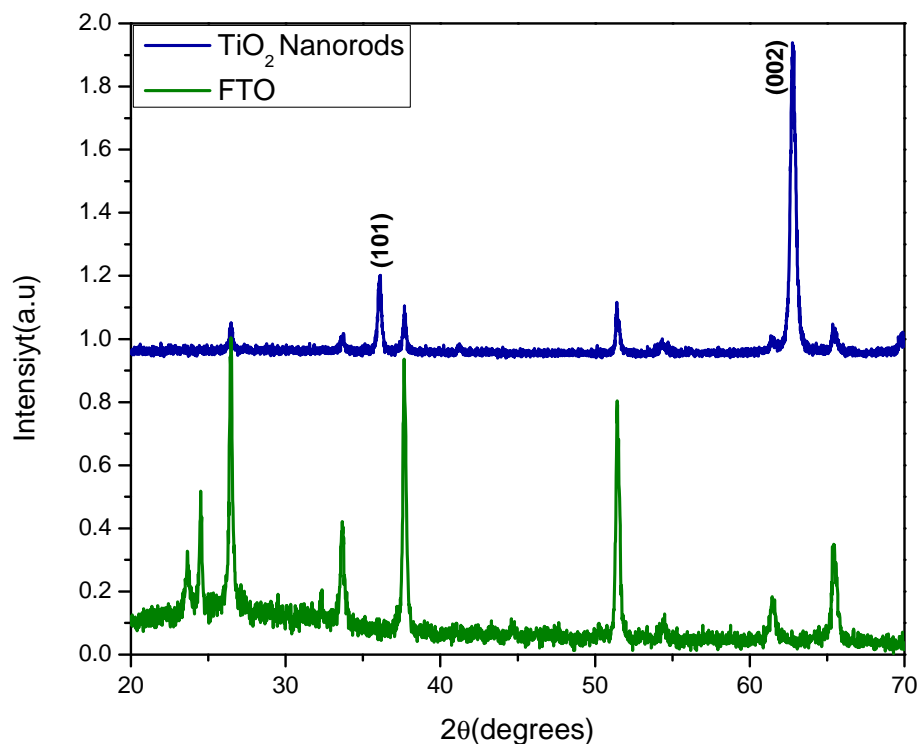


Figure 4.3: XRD pattern of TiO₂ (Rutile Phase) Nanorods

The crystal structure of the as-prepared film was examined by X-ray diffraction (XRD). The XRD patterns were recorded in a Rigaku SmartLab, Automated Multipurpose x-ray Diffractometer with Cu K α radiation (λ) = 0.154 nm) from 20° to 70°. Figure 4.3 shows the XRD patterns of the TiO₂ and FTO substrate nanorods deposited by hydrothermal method at temperature 150°C and annealed at 450°C temperature. All major XRD peaks of the films can be indexed to the rutile phase of TiO₂ (space group $P4_2/mnm$) suggesting that all the films are phase pure except few low intensity peaks nearby $2\theta=36.06^\circ$ and $2\theta=62.76^\circ$, observed for TiO₂ films which corresponds to the FTO substrate peak. The XRD pattern shows (002) as the high intensity peak in the sample, which suggests that films are mostly oriented along (002) plane. The values are confirmed with JCPDS Card No(88-1175)

4.1.4 TEM analysis of TiO₂ Nanorods

The morphology of the film and structure of the nanorods was examined using transmission electron microscopy (TEM) and high resolution TEM (HRTEM) analysis. We observe from Figure 4.4 (b) that nanorods growth is along two planes [110] and [002]. Figure 4.4(a) shows TEM micrograph which confirms the formation of rod like structure in the TiO₂ film. HRTEM image Figure 4.4(b) of the same film indicates clear lattice fringes with d-spacing of 1.49 nm and 2.5 nm, corresponding to the (002) and (101) lattice plane respectively of tetragonal rutile phase TiO₂ clearly indicating the formation of rutile phase. HRTEM image in Figure 4.4(a) clearly indicates the formation of crystalline TiO₂ nanorods along the entire length. The width of nanorod is calculated to be 140 nm.

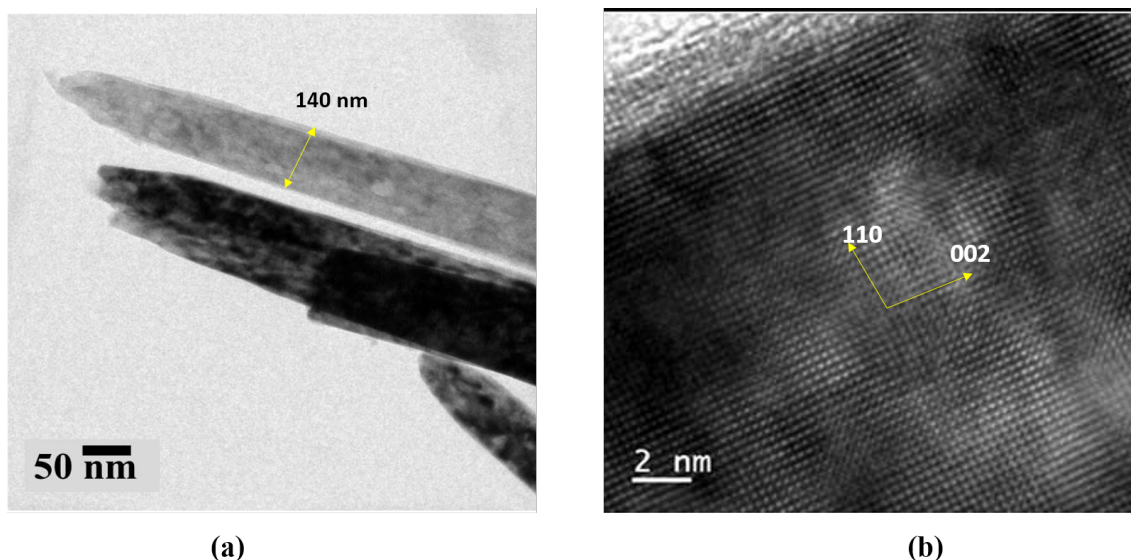


Figure 4.4: (a) TEM image of TiO₂ Nanorod (b) Surface Morphology

4.1.5 SAED analysis of TiO₂ Nanorods

SAED analysis shows that the prominent planes in the TiO₂ rutile phase nanorods are [002] and [110]. This also confirms the XRD analysis done of the single crystal TiO₂ nanorods.

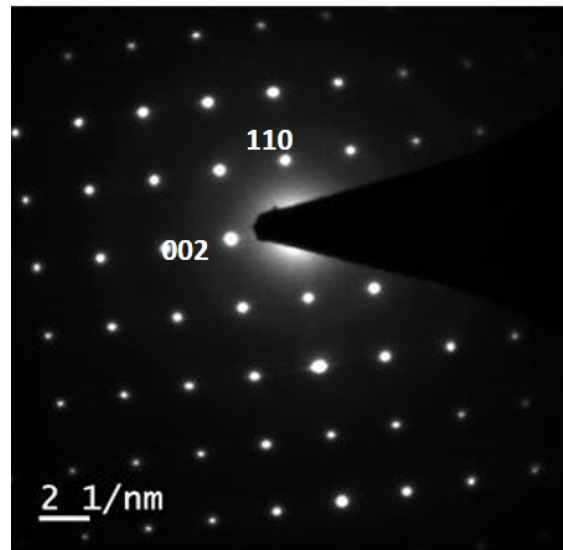
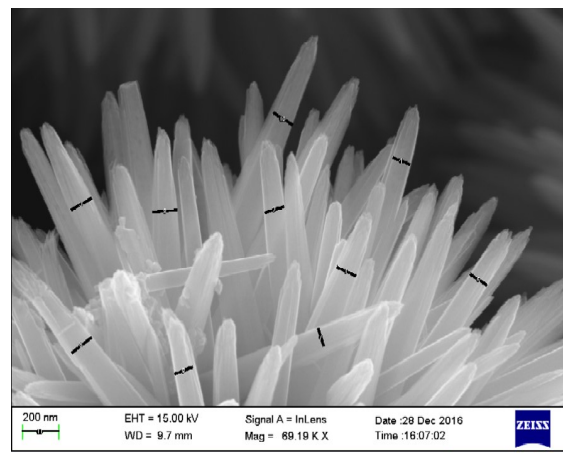


Figure 4.5: (a)

4.1.6 FE-SEM of TiO₂ Nanorods

FE-SEM analysis is done on Field-Emission Scanning Electron Microscope (FE-SEM), Supra55 Zeiss. In Figure 4.7 we observe the formation of nanorods normal to the FTO surface. FE-SEM is done in different locations of the film and it confirms the formation of nanorods on the entire surface of the substrate. It also shows the formation of nanoflower like structure in some parts of the film. The top view of the film confirms that nanorods formed are of tetragonal shape with square top. In Figure 4.6 we calculated the average width of nanorods in the nanoflowers to be 114 nm.

Figure 4.6: Nanorods of average width 114.24 nm in the TiO₂TiO₂ Nanorods

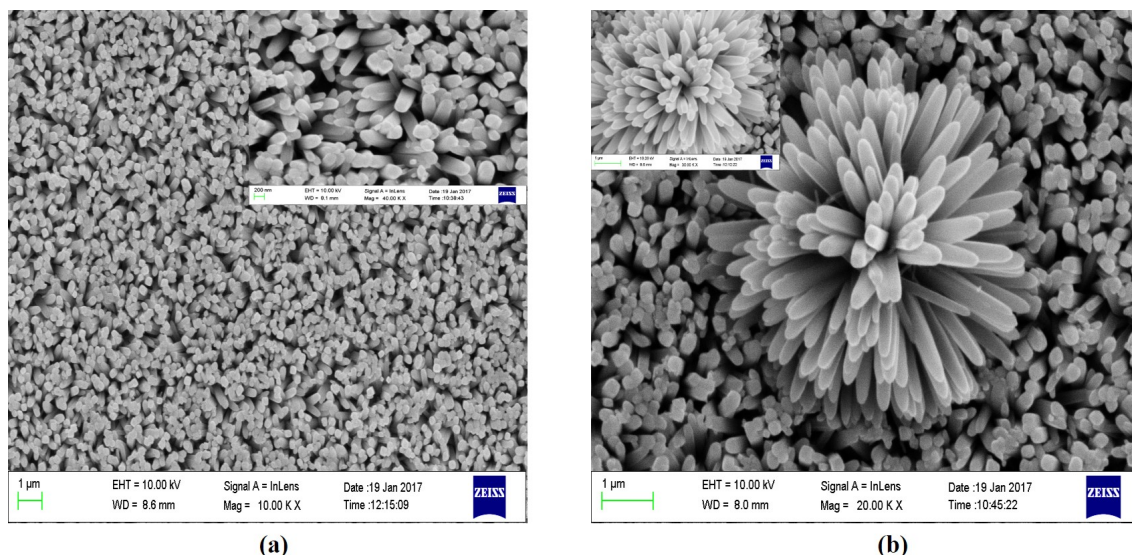


Figure 4.7: SEM image of TiO₂ (rutile phase) Nanorod (a) Morphology of film on FTO (b) Flower like structure made of nanorods

4.2 Light Harvesting Layers

4.2.1 XRD analysis of CH₃NH₃I and (CH₃NH₃)₃Bi₂I₉

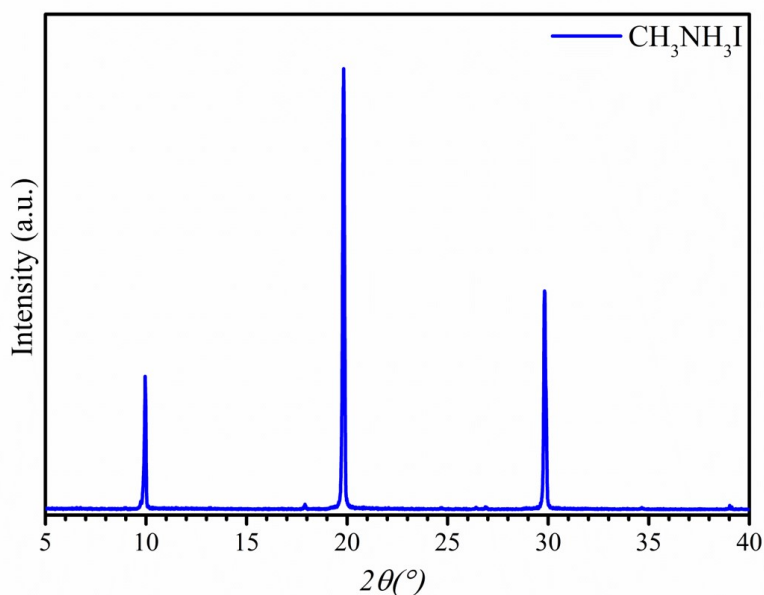


Figure 4.8: XRD Pattern of CH₃NH₃I

The XRD patterns were recorded in a Rigaku SmartLab, Automated Multipurpose x-ray Diffractometer with Cu K α radiation (λ) = 0.154 nm) from 5^o to 40^o. The pattern obtained was similar to the XRD graph in [28]. Crystal structure of the (CH₃NH₃)₃Bi₂I₉ perovskite was determined from XRD measurements, as shown in

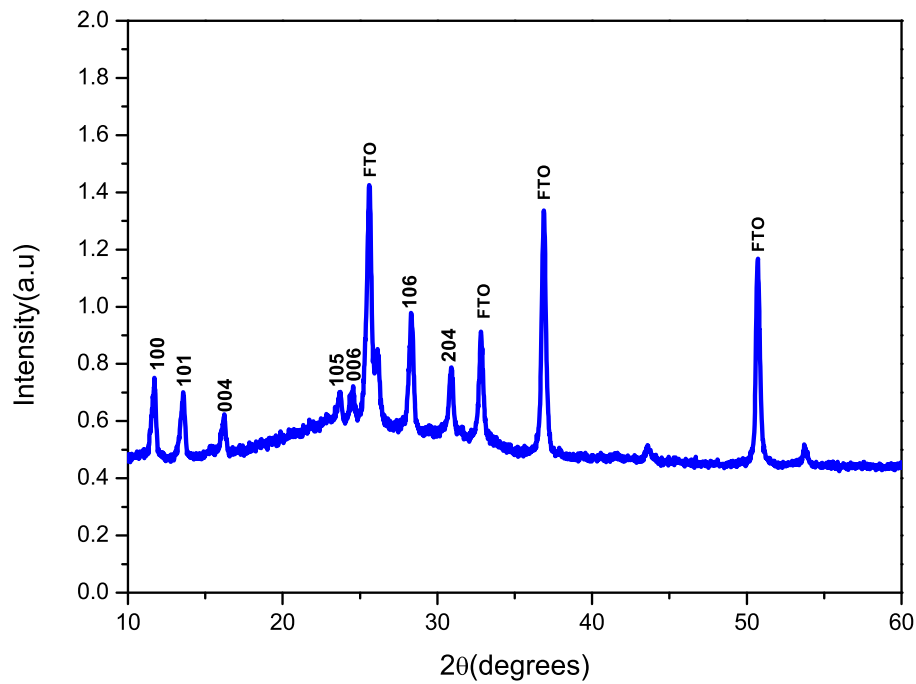


Figure 4.9: XRD Pattern of Bismuth based Perovskite $(\text{CH}_3\text{NH}_3)_3\text{Bi}_2\text{I}_9$ TiO_2 Nanoparticles

Figure 4.9. The diffraction peaks match with the literature values[26], which were solved in the $P6_3/mmc$ space group. The crystalline phases of $(\text{CH}_3\text{NH}_3)_3\text{Bi}_2\text{I}_9$ perovskite are reported in two investigations Szklarz *et.al.* reported that $(\text{CH}_3\text{NH}_3)_3\text{Bi}_2\text{I}_9$ has an orthorhombic structure with $\text{Cmcm}(63)$ space group. However, Jakubas and Sobczyk ref[29] proposed that the crystalline structure is hexagonal with $P6_3/mmc$ space group, similar to the $\text{Cs}_3\text{Bi}_2\text{I}_9$ perovskite. The $(\text{CH}_3\text{NH}_3)_3\text{Bi}_2\text{I}_9$ perovskite we obtained agrees with the results from Jakubas *et.al.* As we have spin coated $(\text{CH}_3\text{NH}_3)_3\text{Bi}_2\text{I}_9$ film on FTO glass we also observe FTO peaks at 2θ values 25.66° , 32.85° , 36.88° and 50.741° .

4.2.2 FE-SEM of $(\text{CH}_3\text{NH}_3)_3\text{Bi}_2\text{I}_9$

FE-SEM images of the film deposited on FTO is shown in Figure 4.10, it shows that the substrate is covered homogeneously by the film. Analysis of the same samples by FE-SEM at $20\mu\text{m}$ shows the hexagonal structure of the material through the formation of hexagonal-shaped edges and crystal. Dimensions of the hexagonal crystal are shown in Figure 4.10(b). The SEM analysis is confirmed from the reported article[30]. The FE-SEM analysis confirms the XRD analysis done above using space group($P6_3/mmc$)

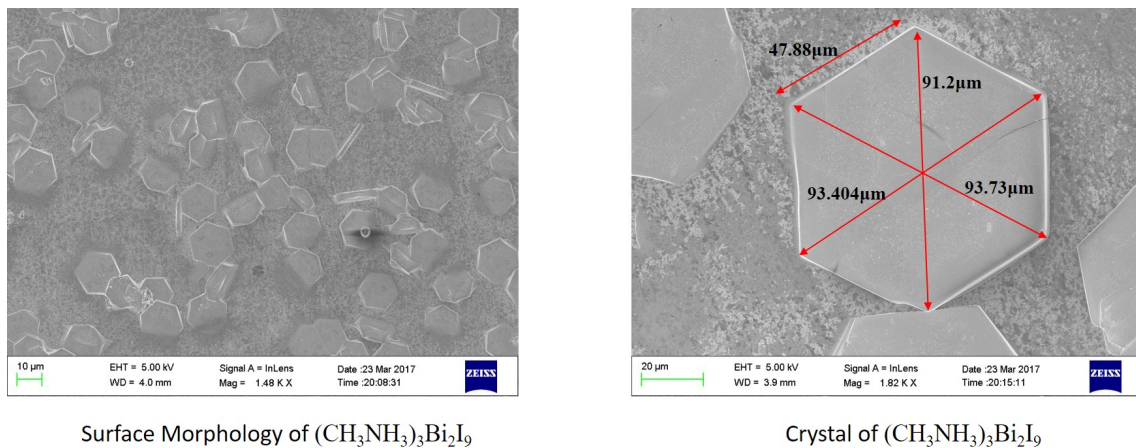


Figure 4.10: FE-SEM analysis of $(\text{CH}_3\text{NH}_3)_3\text{Bi}_2\text{I}_9$ (a) Surface Morphology of Bismuth based perovskite (b) Dimensions of hexagonal plate

4.2.3 Efficiency Calculation of Solar Cells

Here we calculated the efficiency of solar cell with MAPI perovskite as light harvester. The structure of solar cell fabricated by us is shown in Figure 4.11. Here ETL is rutile phase TiO_2 nanorods and HTM is Spiro-MeOTAD. The solar simulation of all photovoltaic devices was done in the Newport Portable Solar Simulator in 1 sun illumination ($\text{AM } 1.5 \text{ G}, 100 \text{ mW cm}^{-2}$) connected to Keithley 2401 source meter. This solar cell with $\text{CH}_3\text{NH}_3\text{PbI}_3$ as light harvesting layer has the active area of 0.25 cm^2 . Here we observe in graph 4.12(a) $J_{\text{SC}}=6.81 \text{ mA cm}^{-2}$ and $V_{\text{OC}}=0.46$ volts and the efficiency of 1.45% with $\text{FF}=46\%$. Another graph 4.11(b) is of Power density v/s Voltage, from this graph we calculated maximum power corresponding to a particular voltage value.

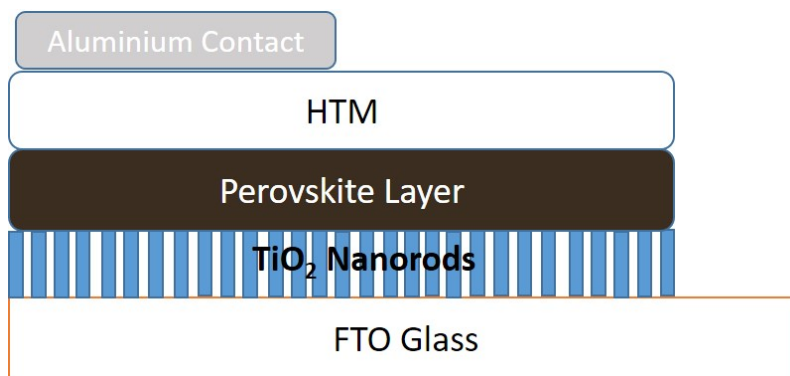


Figure 4.11: Structure of Solar Cell

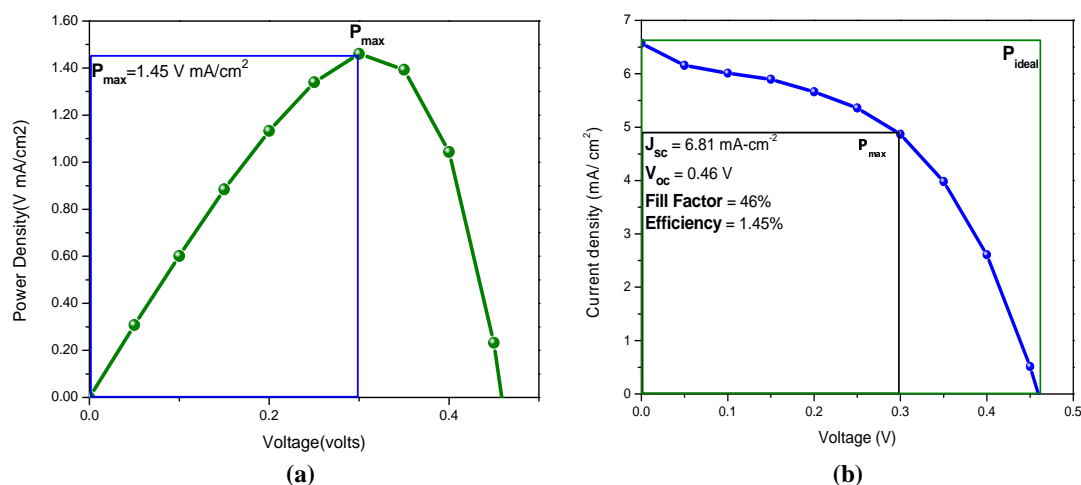


Figure 4.12: Efficiency calculations of solar cell with MAPI as light harvester (a) Power Density Graph (b) J-V graph of solar cell

Reasons for Low Efficiency of Cell

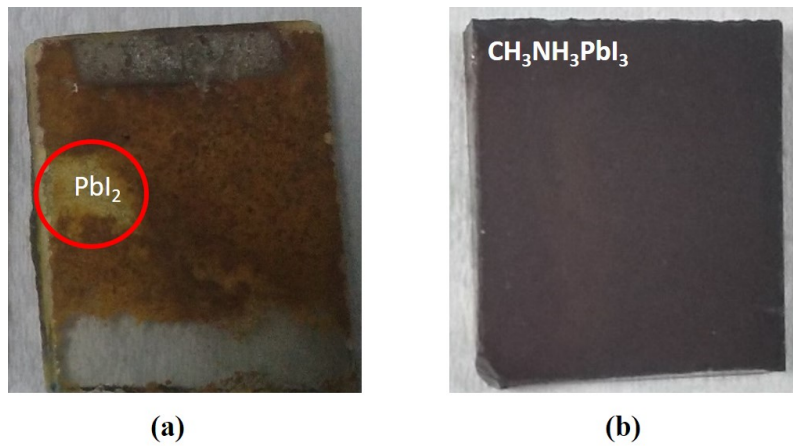
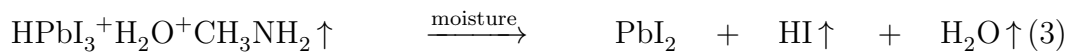
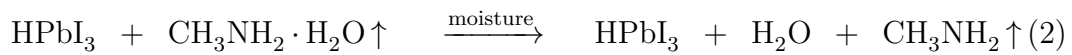
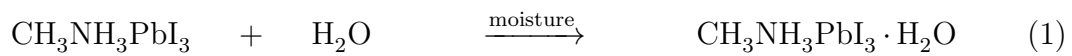


Figure 4.13: (a) Presence of PbI_2 after degradation (b) $\text{CH}_3\text{NH}_3\text{PbI}_3$ Perovskite on FTO/ TiO_2

1. **Preparation of $\text{CH}_3\text{NH}_3\text{PbI}_3$ perovskite in ambient conditions-** As reported earlier and shown in Figure 4.13 that perovskite degrades very fast without vacuum, here also we saw the degradation of film in one day[31]. This happens due to chemical reaction in presence of humidity.



2. **Fabrication of Electrode-** The contacts made may be not able to collect charges as efficiently as expected due to mismatch of energy levels or due to thickness of contact layer.
3. **Solvents added in the HTM-** It as a possible reason that the ratio of solvents used to spin coat HTM layer is a hindrance in the flow of holes through the HTM layer to the contact.
4. **Thermal instability of Perovskite-** We know that perovskite is not stable at high temperatures and it is a possibility that during further processes temperature may have increased therefore making light harvesting layer unstable and reducing the efficiency.

Another device with the structure as shown in Figure 4.14 was fabricated. It has MABI perovskite as the light harvesting layer, ETL is rutile phase TiO_2 nanorods and HTM is Spiro-MeOTAD. In the Figure 4.15 two graphs are shown, first graph is the power density v/s Voltage and second one is J v/s V graph. The simulation of these devices was done 1 week after the fabrication process to compare the change in efficiency with the reported results in [10]. We found that efficiency of solar cell was 0.124% after 1 week of fabrication which is less than the reported efficiency of 0.22%.

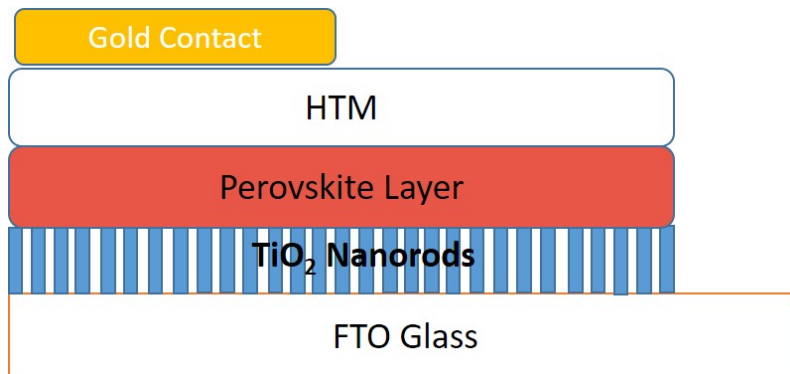


Figure 4.14: Structure of Solar Cell

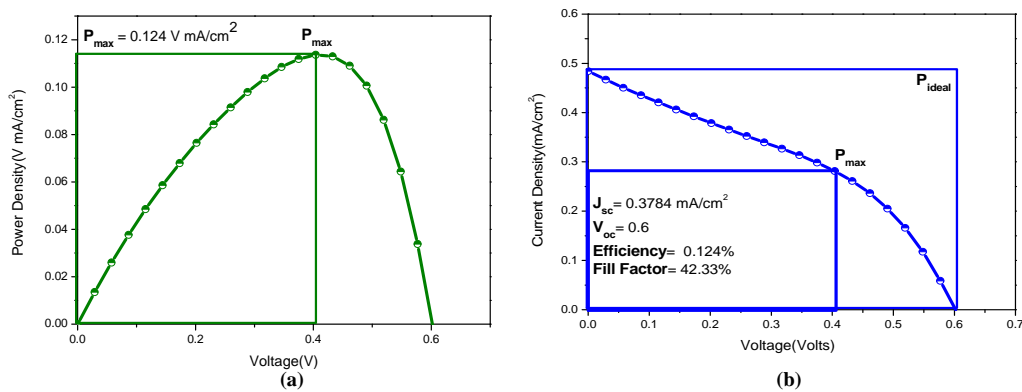


Figure 4.15: Efficiency calculations of solar cell with MABI as light harvester (a) J - V graph of solar cell (b) Power Density Graph

Chapter 5

Summary, Conclusions and Future Scope

5.1 Summary and Conclusions

In summary we have shown synthesis of anatase phase of TiO_2 by sol-gel method using titanium butoxide as precursor. XRD and FE-SEM analysis were done to confirm the anatase phase and nanoparticle formation. We also synthesised TiO_2 film on FTO by hydrothermal process. The phase of nanorods was confirmed by XRD, HRTEM and SAED analysis which showed that growth of nanorods was mainly along [002] plane and of rutile phase. FE-SEM analysis showed the nanorod structure which was tetragonal in shape with square head and of width 114 nm. Methylammonium iodide was synthesised and its XRD was done and compared with the reported results which showed that pure phase MAI was synthesised. $\text{CH}_3\text{NH}_3\text{PbI}_3$ was spin coated on TiO_2 film by two step method, then HTM layer of Spiro-MeOTAD was also spin coated and then metal electrode of aluminium was deposited by thermal evaporation method. Solar simulation of the solar device with $\text{CH}_3\text{NH}_3\text{PbI}_3$ as light harvesting layer showed efficiency of 1.45% and FF was 46%. Various reasons for the low efficiency are also reported. To overcome the drawbacks of $\text{CH}_3\text{NH}_3\text{PbI}_3$ we investigated another perovskite with Bismuth which reduced the toxicity of lead. The perovskite was synthesised using one step method. XRD analysis was done to confirm the various planes as reported in previous papers. FE-SEM

analysis was done to investigate the morphology of film which showed that hexagonal crystals are formed as also reported previously. The solution of prepared perovskite was spin coated on previously prepared TiO_2 film on FTO. Over this HTM layer of Spiro-MeOTAD was spin coated and then electrode was deposited to complete the device. The device was kept in ambient conditions for 7 days and then solar cell simulation was done which showed efficiency of 0.124% and FF of 42.33%.

5.2 Future Scope

Since the year 2012 perovskite solar cells is one of the most interesting topics of research. Many research groups around the globe are working on this. Main reason for so much interest can be scope of engineering and physics involved in each layer of the cell. This mainly stems from long-range ambipolar charge transport properties, low exciton binding energies, and suitable band gap tuning by managing the chemical composition. Until this year high efficiency upto 22% is obtained and it is expected that in the coming years it will cross the Shockley Queisser Efficiency Limit. Another main factor before commercialisation of these cells is the stability in ambient conditions in presence of humidity and high temperatures. This factor can be addressed by replacing lead with another element which fits the perovskite structure. Doping of perovskites is another option to increase efficiency and stability. The charge flow in HTM can also be increased if solvents used in it increase the hole mobility.

Appendix

Solar Cell Simulation

Theory of Solar Radiation

The energy available from the Sun in the form of light is capable of performing certain reactions which produce energy in return this is evident from photosynthesis. The idea to convert sunlight into utilizable form of energy is the basic concept of the solar cell. The solar cell is an optoelectronic device able to convert light into electric current, both the direct sunlight and also artificial or ambient light. However, the term light is referred here as the electromagnetic radiation emitted by the Sun onto the surface of the Earth. The Sun emits electromagnetic waves all over the spectrum of frequencies like a black body with a calculated temperature of 5777 K. Only a fraction of this radiation reaches the surface of the Earth[32]. The air mass coefficient (AM1.5) is an index used to determine the effective electromagnetic radiation emitted by the Sun at the sea level Figure5.1 The main losses with respect the pristine emission are due absorption by the atmosphere of the Earth. Ozone, water vapour, oxygen and carbon dioxide are the relevant absorbing agents that preclude the ultraviolet (UV) and some parts of the infrared (IR) portions of the solar spectrum. The AM1.5 spectrum represents the maximum amount of energy available for a solar cell to be converted in electrical current. According to the AM1.5 spectrum the maximum irradiance peak is in the visible region, however an ideal solar cell must be able to convert the whole part of the spectrum to maximize the yield of photogenerated current.

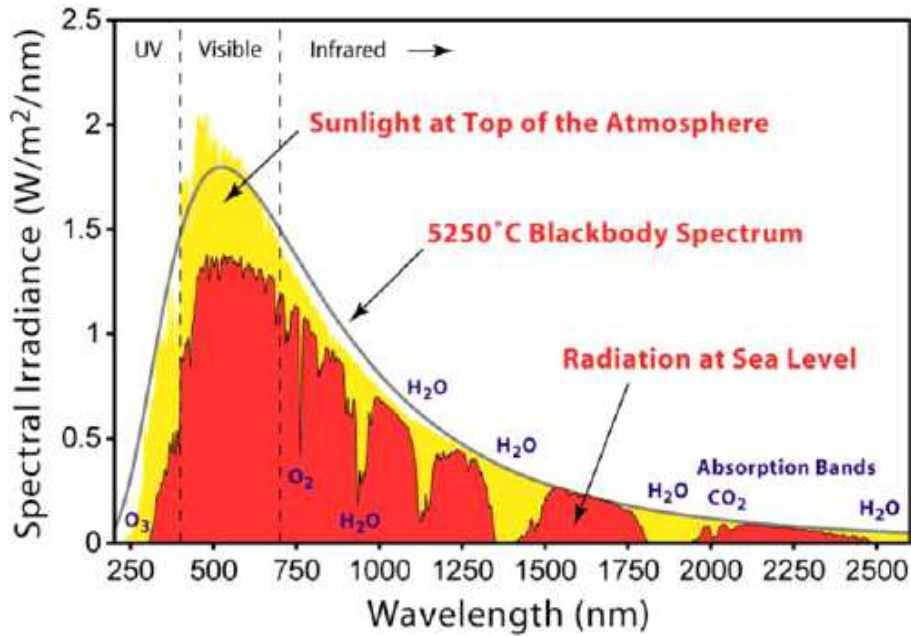


Figure 5.1: Solar irradiance spectrum above the atmosphere and at the surface

Efficiency calculations from J-V Curve

1. Short Circuit Current (I_{SC})

The short circuit current I_{SC} corresponds to the short circuit condition when the impedance is low and is calculated when the voltage equals 0.

$$I \text{ (at } V=0) = I_{SC}$$

I_{SC} occurs at the beginning of the forward-bias sweep and is the maximum current value in the power quadrant. For an ideal cell, this maximum current value is the total current produced in the solar cell by photon excitation.

$$I_{SC} = I_{MAX}$$

2. Open Circuit Voltage (V_{OC})

The open circuit voltage (V_{OC}) occurs when there is no current passing through the cell.

$$V \text{ (at } I=0) = (V_{OC})$$

(V_{OC}) is also the maximum voltage difference across the cell for a forward-bias sweep in the power quadrant.

$(V_{OC})=(V_{max})$ for forward-bias power quadrant

3. **Maximum Power (P_{MAX})** Current at (P_{MAX}) (I_{MP}), Voltage at (P_{MAX}) (V_{MP})

The power produced by the cell in Watts can be easily calculated along the I-V sweep by the equation $P=IV$. At the I_{SC} and V_{OC} points, the power will be zero and the maximum value for power will occur between the two. The voltage and current at this maximum power point are denoted as V_{MP} and I_{MP} respectively.

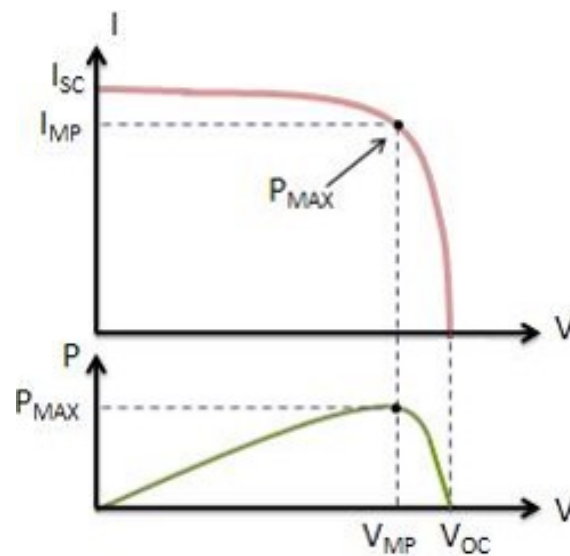


Figure 5.2: MAXimum Power for I-V sweep

4. **Fill Factor (FF)** The Fill Factor (FF) is essentially a measure of quality of the solar cell. It is calculated by comparing the maximum power to the theoretical power (P_T) that would be output at both the open circuit voltage and short circuit current together. FF can also be interpreted graphically as the ratio of the rectangular areas depicted in Figure 5.3 .

$$FF = P_{MAX} / P_T$$

A larger fill factor is desirable, and corresponds to an I-V sweep that is more square-like. Typical fill factors range from 0.5 to 0.82. Fill factor is also often represented as a percentage.

5. **Efficiency (η)**-Efficiency is the ratio of the electrical power output P_{out} , compared to the solar power input, P_{in} , into the PV cell. P_{out} can be taken to be

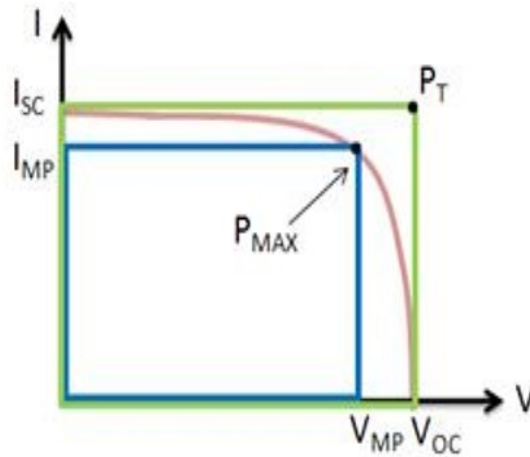


Figure 5.3: FF from I-V sweep

P_{MAX} since the solar cell can be operated up to its maximum power output to get the maximum efficiency.

P_{in} is taken as the product of the irradiance of the incident light, measured in W/m^2 or in suns ($1000 W/m^2$), with the surface area of the solar cell [m^2]. The maximum efficiency (η_{max}) found from a light test is not only an indication of the performance of the device under test, but, like all of the I-V parameters, can also be affected by ambient conditions such as temperature and the intensity and spectrum of the incident light. For this reason, it is recommended to test and compare PV cells using similar lighting and temperature conditions.

$$\eta = P_{out} / P_{in}$$

$$\eta_{max} = P_{max} / P_{in}$$

References

- [1] M. M. Lee, J. Teuscher, T. Miyasaka, T. N. Murakami, and H. J. Snaith, “Efficient hybrid solar cells based on meso-superstructured organometal halide perovskites,” *Science*, vol. 338, no. 6107, pp. 643–647, 2012.
- [2] P. P. Boix, S. Agarwala, T. M. Koh, N. Mathews, and S. G. Mhaisalkar, “Perovskite solar cells: Beyond methylammonium lead iodide,” *The journal of physical chemistry letters*, vol. 6, no. 5, pp. 898–907, 2015.
- [3] U. eia, *International Energy outlook 2017*, <https://www.eia.gov/outlooks/ieo/world.php/>, 2017.
- [4] REN21, *Renewables 2017 global status report*, <http://www.ren21.net/status-of-renewables/global-status-report/>, 2017.
- [5] W. Shockley and H. J. Queisser, “Detailed balance limit of efficiency of p-n junction solar cells,” *Journal of applied physics*, vol. 32, no. 3, pp. 510–519, 1961.
- [6] B. O’regan and M Grätzel, “A low-cost, high-efficiency solar cell based on dye-sensitized,” *nature*, vol. 353, no. 6346, pp. 737–740, 1991.
- [7] A. Kojima, K. Teshima, Y. Shirai, and T. Miyasaka, “Organometal halide perovskites as visible-light sensitizers for photovoltaic cells,” *Journal of the American Chemical Society*, vol. 131, no. 17, pp. 6050–6051, 2009.
- [8] X. Li, D. Bi, C. Yi, J.-D. Décoppet, J. Luo, S. M. Zakeeruddin, A. Hagfeldt, and M. Grätzel, “A vacuum flash-assisted solution process for high-efficiency large-area perovskite solar cells,” *Science*, vol. 353, no. 6294, pp. 58–62, 2016.
- [9] A. M. Ganose, C. N. Savory, and D. O. Scanlon, “Beyond methylammonium lead iodide: Prospects for the emergent field of ns 2 containing solar absorbers,” *Chemical Communications*, vol. 53, no. 1, pp. 20–44, 2017.
- [10] T. Singh, A. Kulkarni, M. Ikegami, and T. Miyasaka, “Effect of electron transporting layer on bismuth-based lead-free perovskite (ch₃nh₃)₃ bi₂i₉ for photovoltaic applications,” *ACS applied materials & interfaces*, vol. 8, no. 23, pp. 14542–14547, 2016.
- [11] B.-W. Park, B. Philippe, X. Zhang, H. Rensmo, G. Boschloo, and E. M. Johansson, “Bismuth based hybrid perovskites a₃bi₂i₉ (a: Methylammonium or cesium) for solar cell application,” *Advanced Materials*, vol. 27, no. 43, pp. 6806–6813, 2015.

- [12] H.-S. Kim, C.-R. Lee, J.-H. Im, K.-B. Lee, T. Moehl, A. Marchioro, S.-J. Moon, R. Humphry-Baker, J.-H. Yum, J. E. Moser, *et al.*, “Lead iodide perovskite sensitized all-solid-state submicron thin film mesoscopic solar cell with efficiency exceeding 9%,” *Scientific reports*, vol. 2, p. 591, 2012.
- [13] J. H. Noh and S. I. Seok, “Steps toward efficient inorganic–organic hybrid perovskite solar cells,” *MRS Bulletin*, vol. 40, no. 08, pp. 648–653, 2015.
- [14] M. A. Green, K. Emery, Y. Hishikawa, W. Warta, and E. D. Dunlop, “Solar cell efficiency tables (version 46),” *Progress in Photovoltaics: Research and Applications*, vol. 23, no. 7, pp. 805–812, 2015.
- [15] U. NREL, *Best efficiency cell review*, <https://www.nrel.gov/pv/>.
- [16] H. J. Snaith, “Perovskites: The emergence of a new era for low-cost, high-efficiency solar cells,” *The Journal of Physical Chemistry Letters*, vol. 4, no. 21, pp. 3623–3630, 2013.
- [17] K. Momma and F. Izumi, “Vesta 3 for three-dimensional visualization of crystal, volumetric and morphology data,” *Journal of Applied Crystallography*, vol. 44, no. 6, pp. 1272–1276, 2011.
- [18] D. Liu and T. L. Kelly, “Perovskite solar cells with a planar heterojunction structure prepared using room-temperature solution processing techniques,” *Nature photonics*, vol. 8, no. 2, pp. 133–138, 2014.
- [19] C. C. Raj and R. Prasanth, “A critical review of recent developments in nanomaterials for photoelectrodes in dye sensitized solar cells,” *Journal of Power Sources*, vol. 317, pp. 120–132, 2016.
- [20] T.-B. Song, Q. Chen, H. Zhou, C. Jiang, H.-H. Wang, Y. M. Yang, Y. Liu, J. You, and Y. Yang, “Perovskite solar cells: Film formation and properties,” *Journal of Materials Chemistry A*, vol. 3, no. 17, pp. 9032–9050, 2015.
- [21] D.-J. Kwak, B.-H. Moon, D.-K. Lee, C.-S. Park, and Y.-M. Sung, “Comparison of transparent conductive indium tin oxide, titanium-doped indium oxide, and fluorine-doped tin oxide films for dye-sensitized solar cell application,” *Journal of Electrical Engineering and Technology*, vol. 6, no. 5, pp. 684–687, 2011.
- [22] T. Dittrich, F. Lang, O. Shargaieva, J. Rappich, N. Nickel, E. Unger, and B. Rech, “Diffusion length of photo-generated charge carriers in layers and powders of $\text{CH}_3\text{NH}_3\text{PbI}_3$ perovskite,” *Applied Physics Letters*, vol. 109, no. 7, p. 073 901, 2016.
- [23] C. Motta, F. El-Mellouhi, and S. Sanvito, “Charge carrier mobility in hybrid halide perovskites,” *Scientific reports*, vol. 5, 2015.
- [24] A. Paulke, S. D. Stranks, J. Kniepert, J. Kurpiers, C. M. Wolff, N. Schön, H. J. Snaith, T. J. Brenner, and D. Neher, “Charge carrier recombination dynamics in perovskite and polymer solar cells,” *Applied Physics Letters*, vol. 108, no. 11, p. 113 505, 2016.
- [25] W.-J. Yin, J.-H. Yang, J. Kang, Y. Yan, and S.-H. Wei, “Halide perovskite materials for solar cells: A theoretical review,” *Journal of Materials Chemistry A*, vol. 3, no. 17, pp. 8926–8942, 2015.

- [26] K. Eckhardt, V. Bon, J. Getzschmann, J. Grothe, F. M. Wisser, and S. Kaskel, "Crystallographic insights into (CH₃NH₃)₃(Bi₂I₉): A new lead-free hybrid organic–inorganic material as a potential absorber for photovoltaics," *Chemical Communications*, vol. 52, no. 14, pp. 3058–3060, 2016.
- [27] J.-H. Im, H.-S. Kim, and N.-G. Park, "Morphology-photovoltaic property correlation in perovskite solar cells: One-step versus two-step deposition of CH₃NH₃PbI₃," *Appl Materials*, vol. 2, no. 8, p. 081510, 2014.
- [28] N. J. Jeon, J. H. Noh, Y. C. Kim, W. S. Yang, S. Ryu, and S. I. Seok, "Solvent engineering for high-performance inorganic–organic hybrid perovskite solar cells," *Nature materials*, vol. 13, no. 9, pp. 897–903, 2014.
- [29] P. Szklarz, A. Pietraszko, R. Jakubas, G. Bator, P. Zieliński, and M. Gałazka, "Structure, phase transitions and molecular dynamics of [C(NH₂)₃]₃[M₂I₉], m = sb, bi," *Journal of Physics: Condensed Matter*, vol. 20, no. 25, p. 255221, 2008.
- [30] M. Abulikemu, S. Ould-Chikh, X. Miao, E. Alarousu, B. Murali, G. O. N. Ndjawa, J. Barbé, A. El Labban, A. Amassian, and S. Del Gobbo, "Optoelectronic and photovoltaic properties of the air-stable organohalide semiconductor (CH₃NH₃)₃Bi₂I₉," *Journal of Materials Chemistry A*, vol. 4, no. 32, pp. 12504–12515, 2016.
- [31] M. Long, T. Zhang, Y. Chai, C.-F. Ng, T. C. Mak, J. Xu, and K. Yan, "Non-stoichiometric acid–base reaction as reliable synthetic route to highly stable CH₃NH₃PbI₃ perovskite film," *Nature Communications*, vol. 7, p. 13503, 2016.
- [32] A. Fahrenbruch and R. Bube, *Fundamentals of solar cells: photovoltaic solar energy conversion*. Elsevier, 2012, pp. 26–31.